Single-crystal X-ray diffraction studies on structural transformations of porous coordination polymers

Journal:	*Chemical Society Reviews*
Manuscript ID:	CS-REV-04-2014-000129.R1
Article Type:	Review Article
Date Submitted by the Author:	02-May-2014
Complete List of Authors:	Zhang, Jie-Peng; Sun Yat-Sen University, School of Chemistry and Chemical Engineering Liao, Pei-Qin; Sun Yat-Sen University, School of Chemistry and Chemical Engineering Zhou, Hao-Long; School of Chemistry and Chemical Engineering, School of Chemistry and Chemical Engineering Lin, Rui-Biao; Sun Yat-Sen University, School of Chemistry and Chemical Engineering Chen, Xiao-Ming; Sun Yat-Sen University, School of Chemistry and Chemical Engineering

SCHOLARONE™
Manuscripts

Journal Name

ARTICLE

Single-crystal X-ray diffraction studies on structural transformations of porous coordination polymers

Jie-Peng Zhang,* Pei-Qin Liao, Hao-Long Zhou, Rui-Biao Lin and Xiao-Ming Chen*

X-ray single-crystal diffraction has been the most straightforward and important technique in structural determination of crystalline materials for understanding their structure-property relationships. This powerful tool can be used to directly visualize the precise and detailed structural information of porous coordination polymers or metal-organic frameworks at different states, which are unique for their flexible host frameworks compared with conventional adsorbents. With a series of selected recent examples, this review gives a brief overview of single-crystal X-ray diffraction studies and single-crystal to single-crystal transformations of porous coordination polymers under various chemical and physical stimuli such as solvent and gas sorption/desorption/exchange, chemical reaction, and temperature change.

1. Introduction

Coordination polymers have been a topical research field in crystal engineering, solid-state chemistry, and materials science for more than two decades, because these compounds can exhibit not only versatile structures, but also unique chemical and physical properties for potential applications. Coordination polymers are one-, two-, or three-dimensional (1D, 2D, or 3D) periodical structures consisting of interconnected organic/inorganic bridging ligands and metal ions/clusters.[1] Compared with other types of molecular materials, coordination polymers sustained by coordination bonds have much higher tendency to form open framework structures robust enough to serve as porous materials. Although porous coordination polymers (PCPs)[2] or metal-organic frameworks (MOFs)[1] are less stable/robust than conventional porous materials such activated carbon and zeolites, their crystalline, diversified, designable, and tailorable structures are highly desirable. The pore size and pore surface of PCPs can be continuously and drastically tuned by deliberate molecule and framework designs.[3-5] Besides porosity, PCPs can also impart other interesting physical properties such as luminescence,[6] conductivity,[7] and magnetism.[8] More importantly, the non-rigid, rotatable, and/or reversible metal-ligand coordination bonds, the weak and changeable supramolecular interactions between multiple coordination networks (either interpenetrated or packed together), and the flexible organic ligands are quite common in PCPs, which generate notable framework flexibility hardly found in inorganic zeolites and carbon materials.[9] These unique characteristics can be used to enhance the performance and/or provide additional functionalities in molecular storage, separation, sensing, and so on.

The structure-property relationship of natural and synthetic materials has always been an important part of chemical researches. Crystalline materials such as zeolites and PCPs are very attractive because the highly ordered, well defined structures not only produce unique properties but also simplify structural characterizations. While a few spectroscopic techniques have been developed to reveal structural information in different aspects and levels,[10-15] crystallography is still the most important and straightforward method for direct visualization of the 3D periodic structures. Since Bragg utilized X-ray diffraction to characterize single-crystal structures of simple salts,[16] this technique has been enormously improved in both hardware and software in the past century. Crystallography is a non-destructive analyzing technique, using either a single-crystal specimen (*ca.* 0.1 mm in diameter or *ca.* 1 μg) or small amounts of microcrystalline powder.

Obviously, microcrystalline powders are generally more available than a single crystal. However, due to the serious overlapping of diffraction peaks, powder X-ray diffraction (PXRD) patterns could only provide much less structural information at less accuracy than for single-crystal X-ray diffraction (SCXRD). Actually, *ab initio* determination of unknown and complicated crystal structures from PXRD data is still a very difficult or even impossible challenge.[17] In contrast, solving structures from SCXRD data has become a quite routine method. SCXRD measured by common in-house X-ray sources can already provide not only precise atomic coordinates, bond lengths and bond angles, but also atomic thermal displacements and occupancies, which are unavailable from PXRD even measured by using highly monochromatized and very intensive synchrotron radiation. Therefore, single crystal is always preferred for determination of crystal structures.

The high-resolution crystal structures are critical for determining the precise atomic positions, so that pore size, pore shape, and pore surface structures of PCPs can be obtained to understand the adsorption properties. Due to the remarkable

framework flexibility, adsorption/desorption and other external stimuli may induce non-ignorable structure transformations for PCPs. First, crystal structures of the as-synthesized adsorbents are generally used as the fundamental information for understanding their properties. However, the host-framework structures of the as-synthesized and activated PCP crystals may be not the same. PXRD using in-house X-ray source is a common, convenient, and acceptable tool to identify and compare the crystallinity, phase purity, and large lattice distortions of the as-synthesized and activated PCPs. However, common samples and PXRD data usually suffer from preferred orientation, low resolution and poor intensity, and peak overlap, which hamper observation of small changes of the atomic positions and/or functional groups that may play important roles on the properties. Therefore, determination of the single-crystal structure of a guest-free or activated PCP is very meaningful. Nevertheless, depending on the guest type and loading, the framework structure of a PCP can further change during the adsorption process. In fact, even for rigid frameworks, single-crystal structures of the guest-loaded materials are also very helpful to directly visualize the host-guest and guest-guest interactions. To fully and precisely understand the complicated sorption mechanism, measuring multiple single-crystal structures at different guest-loading states is a very good approach. Nevertheless, when the crystal size is too small and/or the sample is amorphous, PXRD and other characterization methods may also provide useful information.[18]

A perfect crystal never exists, since crystal growth and post-synthetic treatment always produce defects and damages. Due to the tension and shear forces produced by component changes, the fragile single crystal tends to increase mosaicity and even crack into smaller pieces after guest desorption/adsorption and other post-synthetic treatments. Such phenomena may become more serious for many flexible PCPs exhibiting very significant structural changes. Therefore, single-crystal to single-crystal (SCSC) transformation is rarely observed and of particular interest and importance.[19-23] In principle, a smaller specimen and slower change are beneficial to maintain the single-crystallinity of the sample. Fortunately, commercial single-crystal X-ray diffractometers are equipped with more and more sensitive detectors and high-flux X-ray sources, as well as wide-operating-range temperature-controlling devices for *in-situ* activation and measurement. Actually, SCXRD characterization of PCPs during/after the change of guest-loading and under other chemical/physical stimuli has served as a fundamental approach for studying the interesting properties of these materials.

While several excellent review articles discussing the significant framework flexibility, drastic SCSC structural transformation, and/or solid-state reactivity of porous and nonporous coordination polymers have been published in recent years,[19-27] this review focuses mainly on the role and challenge of SCXRD for the studying the structural transformations of PCPs with representative and recent examples. Based on the origins/mechanisms, *i.e.* change of solvent guest, change of gaseous guest, post-synthetic modification, and physical stimuli, we categorize the structural transformations into four types. Structural transformations of PCPs are commonly induced by the changes of the species and/or loading amounts of guests, in which the chemical compositions of the PCP crystals are altered without chemical reaction on the host frameworks. Since the magnitudes of structural transformations and

difficulties of structural characterizations are significantly different between solvent and gaseous guest molecules, they are discussed in two separated sections. In contrast, PCP crystals can be post-synthetically modified by chemical reactions in the covalent and/or coordination means, in which not only crystals but also the host frameworks change their chemical compositions and structures. Finally, structural transformations of PCPs can be purely induced by physical stimuli such as temperature, in which the chemical compositions of the crystals are unchanged.

2. Structural transformation induced by the change of solvent guest

SCSC transformations of PCPs are mostly induced by desorption, adsorption, or exchange of solvent molecules.[28, 29] An open framework is usually not the most thermodynamically favoured one among all reaction products.[30] Templates, generally solvent molecules used in the synthesis, are included in the as-synthesized PCP crystals to stabilize the open framework structures. When the guest molecules are evacuated from the as-synthesized crystal, the coordination network may collapse irreversibly to form a nonporous structure, remain unchanged, or transform to a new structure that can reversibly adsorb/desorb some kinds of guest species. Only for the latter two cases, the crystals can be categorized as genuine PCPs.

Because of the relatively high boiling points and large molecular sizes, solvent/template molecules interact strongly with the host framework. Some solvent molecules can even coordinate with the metal ions to become a part of the host framework. The changes of such strong host-guest interactions, especially removal of the coordinated solvent molecules, could have a great possibility to induce a significant structural transformation. When the structural change is large enough, it can be easily noticed during routine PXRD characterizations. In some cases, reliable unit-cell volume and symmetry of the new phase can be obtained from high-quality PXRD patterns. Nevertheless, a precise crystal structure of the new phase is more useful for understanding its properties, which encourages many efforts to achieve a SCSC process to enable SCXRD measurement of the activated crystal. Depending on the role of solvent molecule and the degree of structural alternation, we categorize representative examples into the following four types.

2.1 Topology alternation induced by the change of coordinated solvent molecule

Metal ions and ligand donor atoms generally have a finite number of preferred coordination numbers and geometries. Except a few cases such as the elongated octahedral and square-planar Cu(II) ions, the maximum coordination number and corresponding geometry of a metal ion is much more stable than the lower ones. When a donor atom leaves the metal ion, an outer sphere donor would try to approach the vacant coordination site to maintain the original coordination number and geometry. In the restricted crystalline networks, such ligand replacement process is much more difficult than in the solution states, but still frequently observed for coordination frameworks.[31-37] To compensate for the removal of coordinated solvent molecule, the incoming ligand may come from another coordination network in the same crystal, which generates a

new framework connectivity. Usually, this leads to increase of the network dimensionality or complexity.

Kitagawa *et al*. described a series of reversible topochemical transformations between 2D and 3D coordination polymers induced by removal/addition of coordinated solvent molecules.[37-39] For example, heating the single crystal of a 2D framework $[Ln(tci)(H_2O)_2]\cdot 2H_2O$ (Ln = Ce or Pr, H_3tci = tris(2-carboxyethyl)isocyanuric acid) at 80 ^{o}C can remove all H_2O molecules to give a 3D framework $[Ln(tci)]$ (Fig. 1).[37] The vacant sites produced by removal of two coordinated H_2O molecules were occupied by two carboxylate oxygen atoms from another layer. The dehydrated product can adsorb H_2O molecules to transform back to the as-synthesized compound, but it is inert to gases and organic solvents. The flexible ligand and lanthanide metal ions with high coordination numbers were believed to provide structural freedom to facilitate such a significant structural transformation.
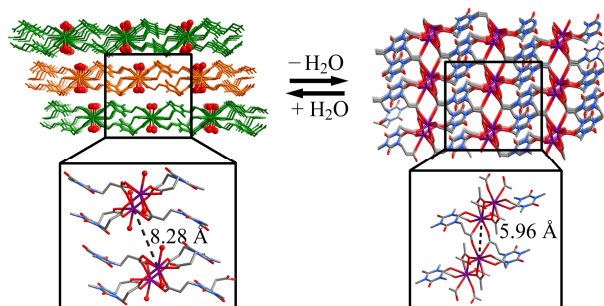
Fig. 1 Interconversion between 2D $[Ln(tci)(H_2O)_2]\cdot 2H_2O$ (Ln = Pr or Ce) and 3D $[Ln(tci)(H_2O)_2]\cdot 2H_2O$ induced by removal and restoration of coordinated H_2O molecules (highlighted as spheres). Hydrogen atoms and lattice H_2O molecules are omitted for clarity. The shortest interlayer metal···metal separations are shown for comparison.
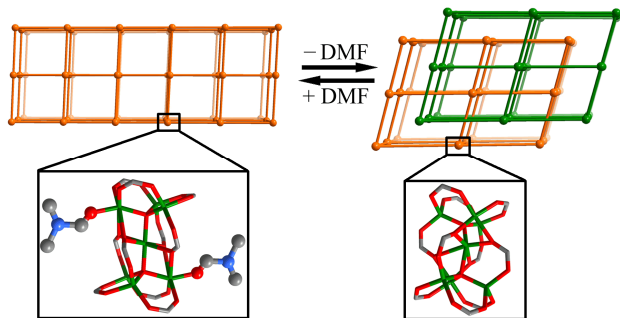
Fig. 2 Interconvertion between non-interpenetrated MOF-123 and 2-fold interpenetrated MOF-246 induced by removal and restoration of coordinated DMF molecules (highlighted in the ball-and-stick mode). Hydrogen atoms are omitted for clarity.

The removal/addition of coordinated solvent molecules may change the interpenetration number of PCPs. For example, Kim *et al*. showed that heating a 3D PCP $[Zn_7O_2(nbd)_5(DMF)_2]$ (MOF-123; H_2nbd = 2-nitrobenzene-1,4-dicarboxylic acid; DMF = *N,N*-dimethylformamide) with non-interpenetrated **pcu** topology can remove the coordinated DMF to form a nonporous crystal $[Zn_7O_2(nbd)_5]$ (MOF-246) with 2-fold interpenetrated **pcu** topology (Fig. 2).[40] The colour, morphology and size of the crystal change obviously

(contracted by *ca*. 50% in thickness) in such a transformation. The reversed transformation can be furnished by soaking the crystal MOF-246 in DMF at 180 ^{o}C. A possible SCSC transformation mechanism was proposed. After removal of the coordinating DMF molecules, the Zn_7O_2 coordination sphere is distorted, which forces half of the nbd^{2-} linkers to leave the Zn_7O_2 units, forming layered fragments. And then, each layer slides into the pore of the neighbouring layer to reduce the empty space. Finally, each layer connects to two next nearest neighbours by the unsaturated Zn_7O_2 units and nbd^{2-} ligands, generating the interpenetrated structure.

Besides removal/addition of coordinated solvent molecules, the network topologies of the host frameworks can be also altered by solvent exchange at the coordination sites. Lin *et al*. reported a 2D PCP $[Zn_2(mtc)(DMF)_4]\cdot 2DMF\cdot 4H_2O$ (H_4mtc = methanetetra(biphenyl-*p*-carboxylic acid)) with 4-fold interpenetrated hinged-layer structure and a small BET surface area of 177 m^2 g^{-1}.[41] Soaking the as-synthesized crystal in CH_2Cl_2 at room temperature for 8 hours gave a 3D structure $[Zn_2(mtc)(H_2O)_2]\cdot G$ (G = uncertain guest molecules) with 4-fold interpenetrated **dia** topology and a large BET surface area of 1170 m^2 g^{-1} (Fig. 3). This example is unique as the 2D to 3D structural transformation increases the porosity and sorption capacity. In the 2D phase, each Zn(II) ion is chelated by two carboxylate groups from two bridging mtc^{4-} ligands and two terminal DMF molecules to form a mononuclear connection. The complete exchange of four coordinated DMF molecules by two water molecules reduce the distance between two mononuclear Zn(II) centres, which are bridged by three μ-carboxylate ends into a dinuclear 4-connected node in the 3D phase. To prove the SCSC transformation mechanism in the solvent immersion process, crystals of $[Zn_2(mtc)(DMF)_4]\cdot 2DMF\cdot 4H_2O$ and a Co(II) analogue were soaked in close proximity in CH_2Cl_2 at room temperature. After more than 3 hours, the morphologies of the crystals remained unchanged, and the 2D to 3D structural transformation completely finished. Inductively coupled plasma-mass spectrometry (ICP-MS) analysis of crystals showed that the crystal of $[Zn_2(mtc)(H_2O)_2]\cdot G$ did not contain Co and the Co(II) analogue did not contain Zn.
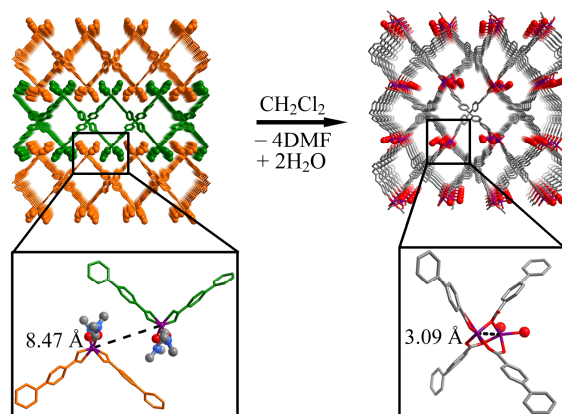
Fig. 3 Conversion of 2D $[Zn_2(mtc)(DMF)_4]\cdot 2DMF\cdot 4H_2O$ to 3D $[Zn_2(mtc)(H_2O)_2]\cdot G$ in CH_2Cl_2 by replacement of coordinated DMF with H_2O molecules (highlighted in the ball-and-stick mode). Hydrogen atoms are omitted for clarity. The shortest interlayer metal···metal separations are shown for comparison.

The bridging ligand can be also replaced by solvent molecules to change its network connectivity. Bu *et al.* reported that when a self-penetrating (3,8)-connected network $[Co_{1.5}(SO_4)(tipb)(bdc)_{0.5}]\cdot 1.75DMF$ (tipb = 1,3,5-tris(pimidazol-ylphenyl)benzene, H_2bdc = 1,4-benzenediarboxylic acid) was exposed to air, the blue crystals gradually turned red without losing single-crystallinity. SCXRD showed that the red crystal possessed a formula of $[Co_{1.5}(tipb)(SO_4)(H_2O)_{3.6}](bdc)_{0.5}\cdot G$, in which the original bdc^{2-} linker left the coordination network, and became a highly disorderd counter anion as confirmed by nuclear magnetic resonance (NMR) and high performance liquid chromatography (HPLC). The H_2O molecule became a terminal ligand, and the Co(II) coordination geometry also changed from tetrahedral to octahedral. Consequently, the host coordination framework was divided into two (3,6)-connected **sit** networks (Fig. 4).[42] On the other hand, activation of the as-synthesized crystal by sequential methanol exchange and heating gave isostructural $[Co_{1.5}(tipb)(SO_4)(bdc)_{0.5}]$ in poor crystallinity.
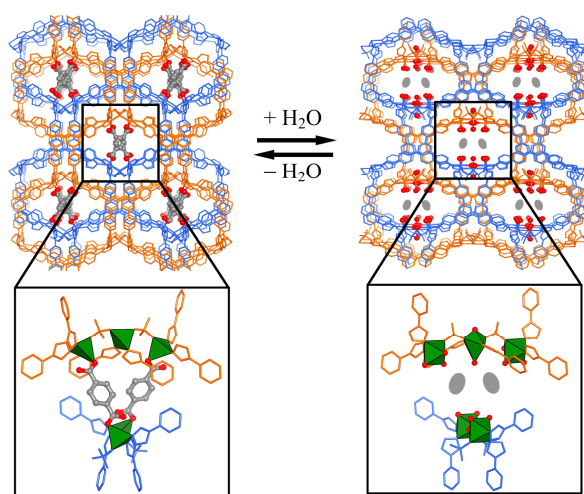
Fig. 4 Interconversion between $[Co_{1.5}(tipb)(SO_4)(bdc)_{0.5}]\cdot 1.75DMF$ and $[Co_{1.5}(tipb)(SO_4)(H_2O)_{3.6}](bdc)_{0.5}\cdot G$ induced by competition between the coordination of H_2O molecules and bridging bdc^{2-} ligands (highlighted in the ball-and-stick mode). Hydrogen atoms are omitted for clarity. The gray ellipses represent disordered bdc^{2-} counter anions not determined by SCXRD.

2.2 Framework distortion induced by the change of coordinated solvent molecule

The long-distance ligand replacement can not occur in many PCPs. For rigid PCPs similar to zeolites, coordinatively unsaturated or open metal sites can be obtained by removal of terminal coordinated solvent molecules. Obviously, open metal sites are energetically unstable, which can be used to strongly bind guests of interests. Nevertheless, to reach the local energy minimum, flexible PCPs tend to distort the whole network and local coordination geometry, or utilize short-distance donors to make the open metal site less open. Compared with examples showing topology alternations, framework distortions induced by the change of coordinated solvent molecules are usually small in extent.[43, 44]

Besides distortion of the whole coordination network, the change of coordinated solvent molecules may induce very significant structural transformations around the coordination center, which can be readily visualized by SCXRD rather than PXRD. For example, Rosseinsky *et al.* reported an interesting reversible ligand substitution SCSC transformation between pink $[Co_2(bpy)_3(SO_4)_2(H_2O)_2]\cdot bpy\cdot CH_3OH$ (bpy = 4,4'-bipyridine) and purple $[Co_2(bpy)_3(SO_4)_2(bpy)(CH_3OH)]$.[45] SCXRD showed that the vacant coordination site generated by removal of the coordinated H_2O molecule was occupied by the lattice MeOH and bpy guests, in which MeOH and bpy molecules moved by 4.4 and 2.8 Å, respectively (Fig. 5). Meanwhile, due to the increased steric requirement of bpy, the coordination network was also distorted slightly, leading to a small change of crystal volume and shape.
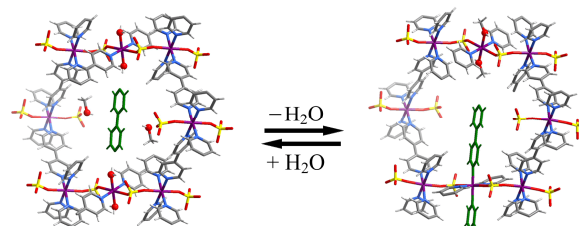
Fig. 5 Interconversion between $[Co_2(bpy)_3(SO_4)_2(H_2O)_2]\cdot bpy\cdot CH_3OH$ and $[Co_2(bpy)_3(SO_4)_2(bpy)(CH_3OH)]$ induced by removal/addition of coordinated H_2O molecules.

In many cases, distortions of the host framework and/or the crystal lattice may be insignificant and even seemingly ignorable.[46-49] For example, a porous magnetic metal carboxylate framework $[KCo_7(OH)_3(ipa)_6(H_2O)_4]\cdot 12H_2O$ (MCF-17; H_2ipa = isophthalic acid) retained single-crystallinity but changed the colour from red to purple after complete removal of both lattice and coordinated H_2O molecules.[50] Although the PXRD patterns of the red and purple crystals are very similar, SCXRD analysis of the purple crystal of $[KCo_7(OH)_3(ipa)_6]$ indicated that their coordination geometries are very different. Most remarkably, a Co(II) ion changed its coordination geometry from an octahedron to a configuration between tetrahedron and distorted trigonal-bipyramid (Fig. 6). When the dehydrated crystal was exposed to air for a few days, the purple crystals returned to red without loss of single-crystallinity. Distortion of the coordination geometry of Co(II) ions and change of coordinated and lattice H_2O molecules significantly switched the magnetic property between spin-canting for the hydrated phase and antiferromagnetism for the dehydrated phase.
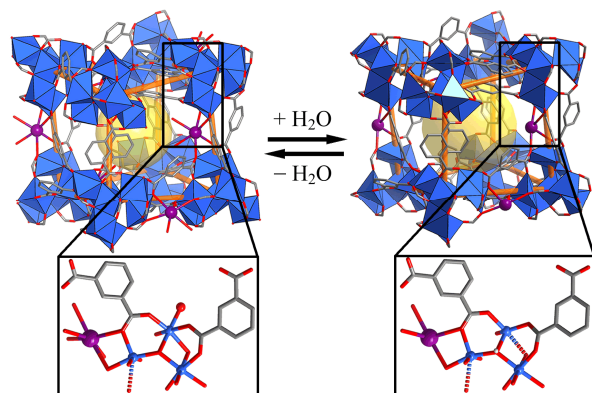
Fig. 6 Interconversion between $[KCo_7(OH)_3(ipa)_6(H_2O)_4]$ and $[KCo_7(OH)_3(ipa)_6]$ induced by removal and restoration of coordinated H_2O molecules. Hydrogen atoms are omitted for clarity.

In another example, there was no visual indication on the colour or PXRD pattern about structural transformation. The single crystal of as-synthesized $[Gd(btc)(H_2O)]\cdot DMF\cdot 0.5H_2O$ (H_3btc = 1,3,5-benzenetricarboxylic acid) always cracked and became opaque by direct heating for guest removal.[51] To facilitate crystal activation, the crystals were exchanged by CH_2Cl_2. The CH_2Cl_2-included crystal became severely and irregularly distorted to form multiple domains, impeding determination of its single-crystal structure. However, high-quality SCXRD data was measured for guest-free $[Gd(btc)]$ obtained by heating the CH_2Cl_2-exchanged crystal at 200 °C for 2 hours, which revealed that the Gd(III) ions were exposed on the channel surface with slightly altered coordination geometry. $[Gd(btc)]$ showed notable selectivity for oxygen-containing solvent molecules. Immersing $[Gd(btc)]$ in EtOH and EtOH-MeCN mixture gave single crystals of $[Gd(btc)(EtOH)]\cdot EtOH$ and $[Gd(btc)(EtOH)]\cdot MeCN$. Interestingly, $[Gd(btc)(EtOH)]\cdot EtOH$ possessed a polar structure (space group $P4_1$), while the guest-free and other solvent-loaded phases were non-polar (space group $P4_122$). Although the unit-cell parameters and PXRD patterns of $[Gd(btc)(H_2O)]\cdot DMF$, $[Gd(btc)(EtOH)]\cdot MeCN$, and $[Gd(btc)(EtOH)]\cdot EtOH$ are very similar, they host frameworks distort very differently (Fig. 7). More importantly, the coordinated EtOH and lattice MeCN molecules could be clearly distinguished in $[Gd(btc)(EtOH)]\cdot MeCN$, demonstrating the oxophilicity of open Gd(III) centres.
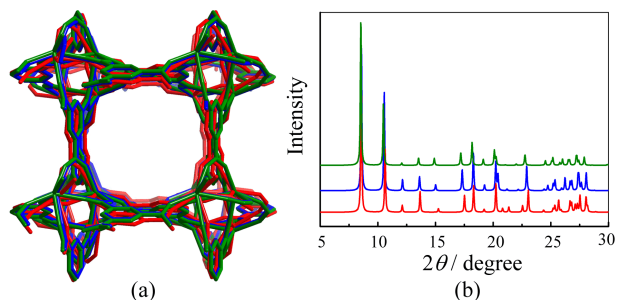
2.3 Topology transformation induced by the change of lattice solvent molecules

Lattice solvent molecules interact with the host framework with hydrogen bonding, π-π stacking and other weak interactions. Removal/adsorption of lattice solvent molecules can hardly change the coordination network topology or connectivity. Available examples,[52, 53] especially occur in the SCSC manner, are still very scarce.

We observed an example of reversible SCSC alteration of interpenetration number in $[Ag_6Cl(atz)_4]OH\cdot nH_2O$ (Hatz = 3-amino-1,2,4-triazole) induced by removal/addition of lattice water molecules.[54] The as-synthesized compound $[Ag_6Cl(atz)_4]OH\cdot 6H_2O$ possessed a cationic framework consisting of two-coordinated Ag(I) ions and three-coordinated triazolate ligands, which interconnected to form 5-fold interpenetrated **dia-f** networks, retaining large 1D channels (diameter $d \approx 8.5$ Å) occupied by counter anions and guest water molecules. Conventional activation led to a shrunk phase with cracked crystals. The single-crystal structure of the shrunk phase was obtained as $[Ag_6Cl(atz)_4]OH\cdot 2H_2O$ by slow and partial dehydration, which revealed not only drastic shrinkage and distortion of the framework and 1D channels (4.3 Å × 10.4 Å), but also a 6-fold interpenetration number (Fig. 8). The Ag(I) ions near the pore surface of $[Ag_6Cl(atz)_4]OH\cdot 6H_2O$ is linearly coordinated, which changed to an obviously bended coordination configuration and formed weak contacts with the remained counter anions and/or lattice H_2O molecules. Based on these structural characters, a possible structural transformation mechanism was deduced, in which the counter anion and/or lattice H_2O coordinated with Ag(I) to form three-coordinated intermediates to facilitate the breakage of Ag(I)-triazolate bonds, and the interpenetration number can be changed by a shift of adjacent connections.
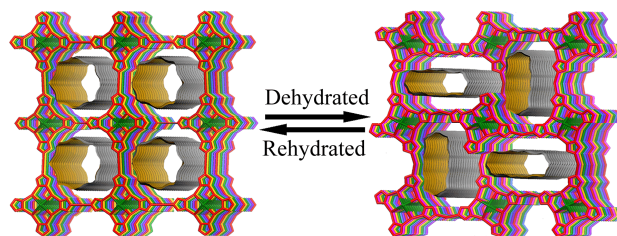
Fig. 8 Interconversion between the 5-fold interpenetrated $[Ag_6Cl(atz)_4]OH\cdot 6H_2O$ and 6-fold interpenetrated $[Ag_6Cl(atz)_4]OH\cdot 2H_2O$ induced by removal and restoration of lattice H_2O molecules (amino groups, counter anion, and H_2O are omitted for clarity, pore surface are highlighted as yellow).

On the other hand, Du *et al*. showed that removing lattice solvent molecules in different routes can lead to completely different types of SCSC transformations.[55] The as-synthesized 3D PCP $[Cu(iba)_2]\cdot 2H_2O$ (Hiba = 4-(1*H*-imidazol-1-yl)benzoic acid) with a 3-fold interpenetrated **lvt** topology can be dehydrated to form two isomeric guest-free phases $[Cu(iba)_2]$ either retaining the original topology or transforming to a 2D **kgm** network (Fig. 9). The former case occurred when the as-synthesized crystal was heated at 160 °C for 12 hours, while the latter case was fulfilled by exposing the as-synthesized crystal in air at room temperature for about two months. The guest-free

(a)

(b)

Fig. 7 Comparison of the (a) coordination frameworks and (b) PXRD patterns of $[Gd(btc)(H_2O)]\cdot DMF$ (green), $[Gd(btc)(EtOH)]\cdot MeCN$ (blue) and $[Gd(btc)(EtOH)]\cdot EtOH$ (red).

lvt framework can be rehydrated to the as-synthesized state, but the **lvt** to **kgm** structural transformation is irreversible.
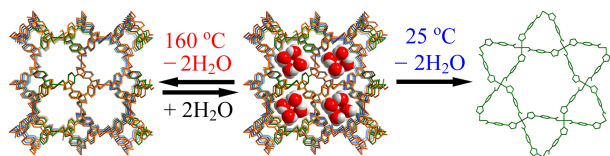
Fig. 9 Conversion of 3D [Cu(iba)$_2$]·2H$_2$O to [Cu(iba)$_2$] isomers either with the original **lvt** topology or a 2D **kgm** topology induced by removing lattice H$_2$O molecules at different temperatures. Hydrogen atoms are omitted for clarity.

In some cases, alteration of the lattice solvent molecules can significantly change the coordination geometry and local connectivity of the building blocks. Kitagawa *et al*. showed that the dinuclear paddle-wheel unit in [Zn$_2$(bdc)$_2$(bpb)]·2.5DMF·0.5H$_2$O (bpb = 2,3-difluoro-1,4-bis(4-pyridyl)benzene) can undergo reversible metal-ligand bond breaking/formation (Fig. 10).[56] Heating the as-synthesized crystals at 115 °C under vacuum gave guest-free [Zn$_2$(bdc)$_2$(bpb)]. SCXRD showed that the coordination environment of the Zn(II) centres changed from square pyramidal to tetrahedral, while one of the two carboxylate groups changed from bidentate to monodentate with the Zn-O distances being changed from 2.043(5) to 5.164(14) Å. As a consequence, the conventional paddle-wheel cluster transformed to an open configuration, although the overall network topology was unchanged. Drastic shrinkage of the unit-cell volume (2070 to 1492 Å^3, 28%) and length of the *c*-axis (18.52 to 14.99 Å, 19%), as well as the solvent accessible volume (40.4 % to 6.5%) were also observed due to the desolvation, which should be the main force for changing coordination topology of the paddle-wheel cluster. By controlled desolvation, two intermediate structures were also obtained and characterized by SCXRD. Interestingly, these transformations can be reversed by Ar, O$_2$, and CO$_2$, as demonstrated by PXRD, Raman spectroscopy, and gas sorption isotherms.
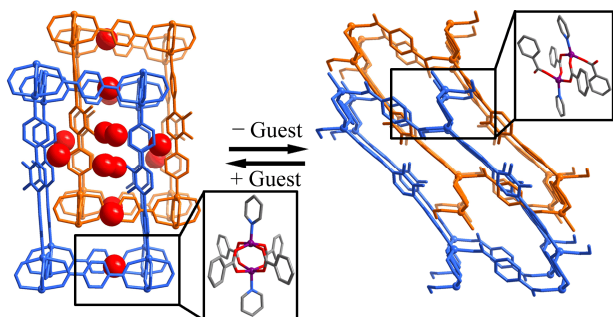
Fig. 10 Interconversion between [Zn$_2$(bdc)$_2$(bpb)]·2.5DMF·0.5H$_2$O consisting of conventional paddle-wheel dinuclear clusters and [Zn$_2$(bdc)$_2$(bpb)] with tetrahedral dinuclear clusters induced by removal and restoration of the lattice solvent molecules (highlighted as spheres). Hydrogen atoms are omitted for clarity.

2.4 Framework distortion induced by the change of lattice solvent molecules

In most flexible PCPs, adsorption/desorption of lattice solvent molecules only distorts the host framework. Without cleavage/formation of coordination bonds, the structural transformation can be still very significant, since framework flexibility is generated by not only the versatile coordination geometries of metal ions but also the rotatable metal ligand bonds, soft organic ligands, and supramolecular packing.

Depending on the topology of the coordination network and flexibility mode of the building blocks, PCPs can show very different types and magnitudes of framework distortion.[57-59] For example, Férey *et al*. developed a highly breathable family of frameworks [M$_3$(μ$_3$-O)(ldc)$_3$(H$_2$O)$_2$(X)]·G (MIL-88s, M = Fe or Cr, H$_2$ldc = linear dicarboxylic acid, X$^-$ = coordinated anion) with a 6-connected **acs** network (hexagonal symmetry) based on trigonal-prismatic nodes and linear dicarboxylate linkers (Fig. 11), in which the framework distortion degrees can be controlled by the length and the substituent group of the linear dicarboxylate, as well as the type of lattice solvent molecules.[60-62] These structures expand by shortening the *c*-axis and simultaneous expanding the *ab*-plane. The largest volumetric and axial breathing amplitudes, 237% and 100%, respectively, were observed in the crystals constructed by 4,4'-biphenyldicarboxylate. Because large crystals can be hardly obtained, these compounds and transformations were mostly studied by PXRD.
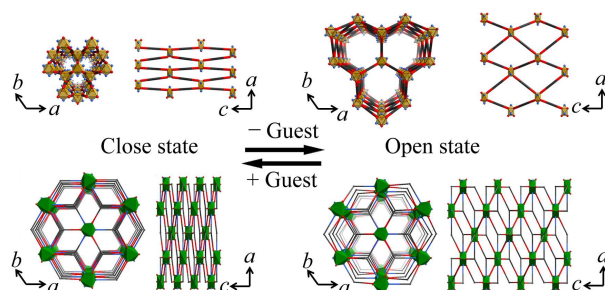
Fig. 11 Comparison of the network topologies and breathing behaviours of MIL-88s and MCF-18.

Subtle modification of the network connectivity may drastically alter the framework distortion mode. Recently, we reported a flexible PCP showing similar network topology but reversed framework breathing direction with MIL-88s. A (3,9)-connected **xmz** (trigonal symmetry)[63] framework [Ni$_3$(μ$_3$-OH)(dcb)$_3$] (MCF-18, H$_2$dcb = 2,6-di-*p*-carboxyphenyl-4,4'-bipyridine) was constructed by trigonal pyridyldicarboxylate ligands and tricapped trigonal-prismatic Ni$_3$(μ$_3$-OH)(RCOO)$_6$(Rpy)$_3$ (RCOO$^-$ = carboxylate group; Rpy = pyridyl group) clusters (Fig. 11).[64] PXRD showed that MCF-18 can drastically swell 70–105% in volume and 75–121% in length upon inclusion of different solvent guests. Because of the restriction on the equatorial sites by coordination of pyridyl ends, MCF-18 distorted almost only at the *c*-axis, giving rise to exceptionally large axial breathing amplitude. The breathing amplitudes of MCF-18 for different solvents followed a sequence similar for MIL-88s. Although single crystals of MCF-18 tended to crack during desolvation and solvent exchange, single-crystal structures were successfully measured for MCF-18, MCF-18·MeOH, MCF-18·DMF, and MCF-18·pyridine, demonstrating that bending of the metal–carboxylate junction and conformational change of the organic ligand were mainly responsible for the breathing behaviour.

The MeOH lattice molecules were highly disordered and could not be modeled, while the DMF guest molecules were relatively ordered and modeled with some geometric restraints. Interestingly, other known coordination polymers with the **xmz** topology (including nonporous and highly porous structures with similar porosity as MCF-18) did not show solvent-induced framework breathing.[63, 65] Detailed comparison showed that the shape of the organic ligand in MCF-18 restricted the $Ni_3(\mu_3\text{-}O/\mu_3\text{-}OH)(RCOO)_6(L^T)_3$ (L^T = terminal ligand) cluster in a geometry that is bendable and requires a reversed bending direction compared with those observed in MIL-88s (Fig. 11).

Pillared-rod structures constructed by inorganic chains and ditopic organic ligands are a typical type of PCPs showing anisotropic framework breathing.[66, 67] For example, Long *et al.* reported a PCP [Cu(bdt)(μ-DMF)]·G (H_2bdt = 1,4-benzenedi(1H-1,2,3-triazole)) showing large fence-like framework breathing controlled by the loading of lattice solvent molecules.[68] In this structure, infinite $Cu(\mu\text{-}DMF)(Rtz)_2$ (Rtz^- = triazolate group) rods were pillared by the linear ligands to form a 3D framework, retaining 1D channels running along the rods. Upon exposure to ambient air, the framework released lattice solvent molecules and underwent two sequential SCSC transformations, changing the unit-cell volume from 2186 Å^3 to 1937 Å^3 and finally to 1567 Å^3, but there was almost no change in the rod direction (Fig. 12). Detailed analyses of single-crystal structures showed that the geometry changes associated with flexing of the bridging ligand was the main reason for the shrinkage of the framework. PXRD showed that the breathing was reversible, but the intermediate state could not be captured.
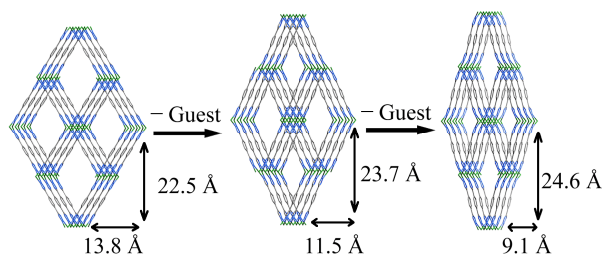
Fig. 12 Multi-step SCSC distortion of [Cu(bdt)(DMF)]·G induced by removal of guest molecules. Coordinated and lattice solvent molecules, as well as framework hydrogen atoms are omitted for clarity.

Huang *et al.* reported a similar multi-step SCSC breathing example in [Zn$_3$(μ$_3$-OH)$_2$(btac)$_2$]·DMF·4H$_2$O (H$_2$btac = benzotriazole-5-carboxylic acid) consisting of infinite zigzag-ladder rod-shape Zn$_3$(μ$_3$-OH)$_2$(RCOO)$_2$(Rtz)$_2$ chains.[69] Interestingly, the Co(II) analogue of this compound is rigid.[70] A converse phenomena was observed in isostructural [Zn(bdp)] and [Co(bdp)] (H$_2$bdp = 1,4-benzenedipyrazole) by Long *et al.* (Co(II) compound possessed much higher flexibility than the Zn(II) analogue),[71, 72] which can be attributed to the stereochemical rigidity of the ZnN$_4$ tetrahedron.[73] These results demonstrate that besides the framework connectivity, local coordination structure and type of lattice solvent, metal ion and amount of lattice solvent are also important parameters in controlling the framework flexibility/rigidity and breathing amplitude.

With isotropic network topologies, the framework distortion manner could be more freely because the anisotropic breathing modes of building blocks are averaged. We have observed different types of framework distortions in a hydrophobic porous metal azolte framework [Cu(detz)] (MAF-2, Hdetz = 3,5-diethyl-triazole), which can shrink, expand, and distort to respond the inclusion of different lattice solvent molecules (Fig. 13).[74] MAF-2 possesses an **nbo**-type coordination framework and a **bcu**-type channel system (the maximum symmetries of **nbo** and **bcu** topologies are cubic). Each aperture between adjacent **nbo** cages are surrounded by six ethyl groups, resulting in a very small effective size ($d \approx 1.5$ Å) in the crystal structure. Room-temperature solvent vapour sorption measurements showed that MAF-2 can adsorb stoichiometric and large amounts of organic solvents MeOH, EtOH, MeCN, and C$_6$H$_6$, but completely exclude H$_2$O and oversized C$_6$H$_{12}$ even close to the saturation vapour pressures. Since the crystallographic aperture size is obviously smaller than the sizes of the adsorbed molecules, the ethyl-blocked apertures have to open, by conformational change of the ethyl groups and even distortion of the Cu(I)-triazolate backbone, for guest diffusion. In principle, conformational change of ethyl groups is enough for passing MeOH, EtOH, MeCN, and smaller guests, and backbone distortion is necessary for benzene but may not enough for larger guests. SCSC transformations were accomplished between the guest-free phase and the MeOH-, EtOH-, and MeCN-included phases, but adsorption of benzene crashed the single crystal of MAF-2, which can be explained by the greater damage induced by backbone distortion.

(a)

(b)

(d)

(c)

(e)
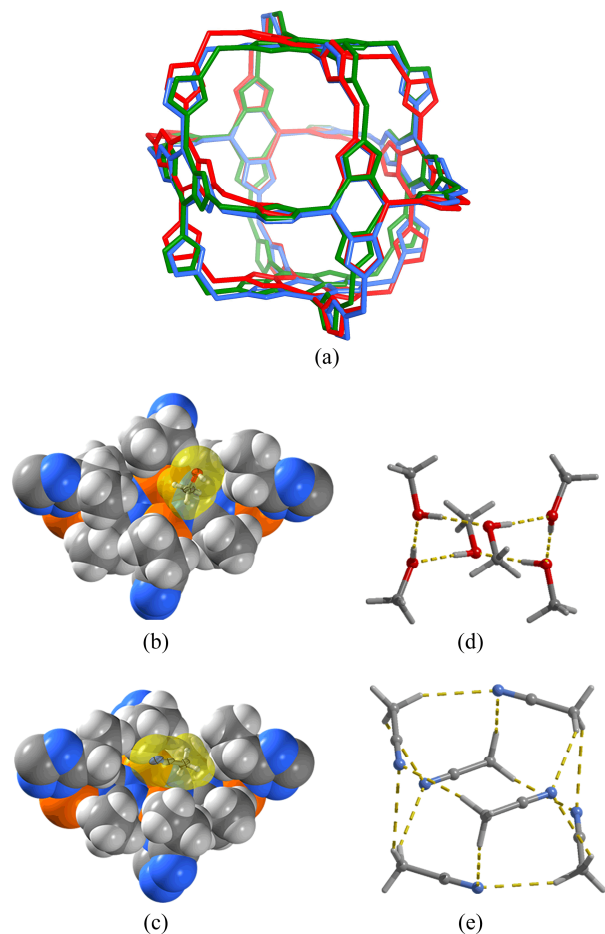
Fig. 13 (a) Comparison of the Cu(I)-triazolate backbones (ethyl groups are omitted for clarity) of guest-free (red), MeCN-included (blue), and C_6H_6-included (green) MAF-2. Local host-guest structures of (b) MAF-2·MeOH and (c) MAF-2·MeCN and supramolecular structures of the (d) MeOH hexamer and (e) MeCN hexamer.

Due to the rotatable coordination bonds, the coordination framework of MAF-2 can distort significantly to adopt different crystal symmetries (Fig. 13). The MeOH- and EtOH-included, and guest-free phases possess the trigonal space group R-3. Inside each **nbo** cage, six alcohol molecules form a chair-like supramolecular hexamer sustained by O-H···O hydrogen bonds (O···O 2.67-2.69 Å). At the same temperature of 123 K, the unit-cell volume of the guest-free phase (4766 Å^3) is 1.8% larger than the MeOH-included phase (4682 Å^3) but 1.1% smaller than the EtOH-included one (4819 Å^3) indicating that MeOH hexamer is smaller than the cavity and attract the host framework to shrink, while the EtOH hexamer is larger than the cavity and expand the framework by steric repulsion. The MeCN-included phase possesses the triclinic P-1 space group, in which the MeCN molecules aggregate with multiple C–H···N interactions (C···N 3.52 Å) to form a unique hexamer with asymmetrically flatten octahedral geometry. Interestingly, the solvent molecules interact with the pore surface with their alkyl groups rather than the more polar hydroxyl or nitrile groups, demonstrating the hydrophobic nature of MAF-2.

Similar to other examples (Fig. 7), SCXRD is necessary for visualizing the small yet important structural transformations occurred for MAF-2. On the other hand, the host framework structure of the benzene-included phase of MAF-2 was deduced from its PXRD pattern, as it is similar to the cubic phase of MAF-2 synthesized by *in-situ* oxidative cycloaddition of propionitrile and ammonia in the presence of Cu(II).[54] According to the benzene sorption isotherm, each **nbo** cage accommodate three benzene molecules, whose location is obviously not compatible with the cubic symmetry.
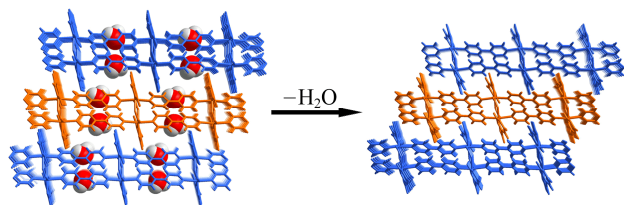
Fig. 14 Sliding of 2D layers of [Fe(pydc)(bpy)] induced by removal of lattice H_2O molecules (highlighted in the space-filling mode).

Besides expansion, shrinkage, and distortion of a single coordination network, interframework sliding between multiple interpenetrated or packed coordination networks can also distort the PCP crystal.[29, 75-79] For example, we reported that a PCP [Fe(pydc)(bpy)]·H_2O (H_2pydc = pyridine-2,5-dicarboxylic acid, bpy = 4,4'-bipyridine) consisting of 2D thick layers can exhibit SCSC sliding of the layers triggered by guest exchange, dehydration, and readsorption (Fig. 14).[79] Activating the as-synthesized crystal [Fe(pydc)(bpy)]·H_2O under a N_2 atmosphere at 160 °C yielded anhydrous [Fe(pydc)(bpy)] with an 8.2% smaller unit-cell volume. Comparison of their single-crystal structures showed that the 2D layers remain almost

unchanged, but their packing mode varied from slightly offset to highly canted stacking.
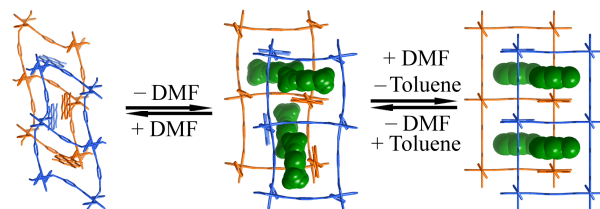
Fig. 15 Interconversion among [Zn$_2$(bdc)$_2$(dpndi)], [Zn$_2$(bdc)$_2$(dpndi)]·4DMF, and [Zn$_2$(bdc)$_2$(dpndi)]·2.5toluene showing single-framework distortion and multi-framework sliding. Hydrogen atoms are omitted for clarity.

More commonly, interframework sliding and framework distortion occur simultaneously.[80] For example, Kitagawa *et al.* reported a flexible PCP [Zn$_2$(bdc)$_2$(dpndi)]·4DMF (dpndi = N,N'-di(4-pyridyl)-1,4,5,8-naphthalenediimide) with 2-fold interpenetrated jungle-gym structure, which showed multimode structural transformation and luminescence responses for aromatic guests.[77] Depending on the type and amount of solvent molecules, the 2-fold interpenetrated coordination networks can change interframework and host-guest interactions significantly by adopting different degrees of network distortion and different mutual positions between the two coordination networks (Fig. 15).

Schröder *et al.* reported a flexible PCP (Me$_2$NH$_2$)$_{1.75}$[In(bptc)]$_{1.75}$(DMF)$_{12}$(H$_2$O)$_{10}$ (NOTT-202, H$_4$bptc = biphenyl-3,3',5,5'-tetra(phenyl-4-carboxylic acid)) with 2-fold interpenetrated 3D binodal 4-connected networks.[81] Upon guest removal, the crystal exhibited an expansion in the unit cell by 11% and solvent-accessible volume by 10% due to framework distortion including an increase of In–O bond length from 2.355(7) to 2.774(3) Å. More interestingly, sliding between the two interpenetrated increased the channel size from 5.0×5.0 to 9.0×9.0 Å^2 (Fig. 16).
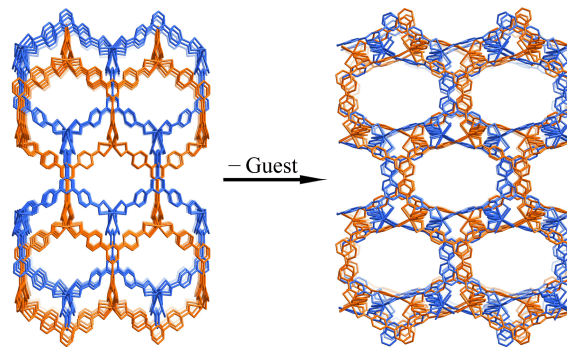
Fig. 16 Single-framework distortion and multi-framework sliding from NOTT-202 to NOTT-202a induced by removal of lattice solvent molecules. Hydrogen atoms are omitted for clarity.
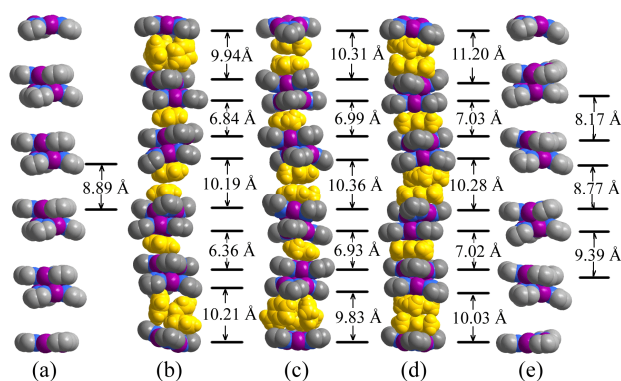
Fig. 17 Comparison of the host-guest structures of (a) $[Ag_2(bpz)]$, (b) $[Ag_{30}(bpz)_{15}]\cdot10C_6H_6$, (c) $[Ag_{30}(bpz)_{15}]\cdot9C_7H_8$, (d) $[Ag_{30}(bpz)_{15}]\cdot8C_9H_{12}$, and (e) $[Ag_{18}(bpz)_9]\cdot xC_9H_{12}$ ($x < 4.8$). For clarity, only the crystallographically resolved lattice solvent molecules (gold) and the $Ag_3(pz)_3$ cores of the host frameworks are shown. Crystallographically independent pore sizes are indicated.

In special cases, interframework sliding and framework distortion occur in very complicated manners. For example, Kitagawa *et al.* reported a highly symmetric porous framework $[Ag_2(bpz)]$ (H_2bpz = 3,3',5,5'-tetramethyl-4,4'-bipyrazole) with 4-fold interpenetrated **srs** topology crystallizing in the cubic space group I-$43d$ ($Z = 48$).[82] In this structure, three Ag(I) ions were coordinated by three pyrazolate moieties to form the classic triangular $Ag_3(Rpz)_3$ (Rpz^- = pyrazolate group) units, which were exposed on the pore surface and suitable to interact with planar aromatic molecules in the face-to-face fashion. Since the two pyrazolate rings in the bpz^{2-} ligand can rotate around their joined C–C single bond, the coordination network was highly distortable. Upon saturated adsorption of benzene (C_6H_6), toluene (C_7H_8), and mesitylene (C_9H_{12}) in the lattice, the crystal transformed to the tetragonal space group $I4_1/a$ ($Z = 16$) with quintuple unit-cell volumes, meaning that their structural complexities were 15 times that of the guest-free phase. The aromatic molecules were sandwiched by pairs of $Ag_3(pz)_3$ units as monomers and different types of dimers and trimers in the very complicated guest-included phases $[Ag_{30}(bpz)_{15}]\cdot10C_6H_6$, $[Ag_{30}(bpz)_{15}]\cdot9C_7H_8$, and $[Ag_{30}(bpz)_{15}]\cdot8C_9H_{12}$. Since the whole crystal showed very small expansion, the simultaneous shrinkage and expansion of pores in different degrees can be regarded as a result of complicated local framework distortion and interframework sliding. Detailed analyses of these crystal structures showed that the bpz^{2-} adopt a variety of conformations (Fig. 17). More interestingly, with partial loading, the single-crystal specimen can reversibly transform to other single-crystalline phases (one of which has been solved by SCXRD although the amount and locations of disordered solvent molecules could not be determined) and even amorphous phase, which further illustrate its robustness and flexibility.[83]

Actually, many flexible PCPs showed reversible crystal-to-amorphous,[84] and even continuous structural transformations from one single crystal to amorphous, and then to another single crystal. In these cases, the amorphous phases should exhibit non-periodical framework distortion rather than framework collapse. For example, Morris *et al.* studied the flexibility of $[Cu_2(OH)(sip)(H_2O)]\cdot2H_2O$ (Cu-SIP-3; H_3sip = 5-sulfoisophthalic acid) using *in-situ* SCXRD at variable

temperature.[85] A series of diffraction data sets were collected for about every 15 K interval from 150 to 500 K, and the occupancies of the three crystallographically independent water molecules were allowed to refine freely. Based on the change of occupancies, partial loss of guest water molecules were observed between 150 and 370 K, during which the host framework show gradual distortion. Above 405 K, the Bragg peaks return and the structure can be refined as the dehydrated phase $[Cu_2(OH)(sip)]$, demonstrating the crystal did not collapse but just lose long-range order at 370-405 K. Between 370 and 405 K corresponding to the removal of other H_2O molecules, no discrete, sharp Bragg peak can be seen by SCXRD. Therefore, the authors utilized the pair distribution function (PDF) method, a total scattering technique that does not require crystalline order to be informative, to visualize the complicated local structural transformations.[18]

Although the structural transformations of PCPs induced by the change of solvent guests are discussed above in four typical types, some PCPs can show two or more types of such structural transformations. For example, Shimizu *et al.* reported a porous metal sulfonate framework showing very interesting multi-step SCSC dehydration.[86] The as-synthesized compound $[Ba_3(H_2O)_6(bts)_2]\cdot8H_2O$ (H_3bts = benzene-1,3,5-trisulphonic acid) can sequentially transform to $[Ba_3(H_2O)_6(bts)_2]\cdot2H_2O$ and $[Ba_3(H_2O)_6(bts)_2]$ by standing in air, and finally to $[Ba_3(bts)_2]$ by heating, during which not only significant framework shrinkage, but also relocation of coordinated H_2O molecules, alteration of coordination numbers, and rearrangement of the coordination connectivity were observed.

3. Structural transformation induced by the change of gaseous guest

Gases, especially permanent gases, have much lower boiling points and smaller molecular sizes than liquid/solvents. Due to the very weak interaction between gas molecules and host framework, gas-induced structural transformations are generally small in extent, but it can be still crucial for the adsorption mechanism. Since most in-house diffractometers are not convenient to measure PXRD for gas-loaded PCPs, gas-induced structural transformations are commonly suggested by abnormal gas adsorption isotherms. Nevertheless, without a gas-loaded crystal structure, the abnormal gas adsorption isotherm can be also explained by relocation and/or layer-by-layer adsorption of guest molecules. Although molecular dynamic calculation is emerging as a powerful tool for simulating the adsorption mechanism,[87-90] measuring the guest-loaded crystal structure is still the most reliable and straightforward approach. Nevertheless, crystal structures of gas-loaded PCPs are still rarely reported. So far most examples are measured by synchrotron and neutron PXRD,[91-95] probably because of the difficulty in preparing single-crystal samples, enthusiasm in hydrogen storage in recent years, and availability of advanced temperature/pressure controlling accessories.

For PCPs with different adsorption sites and/or gas-induced structural transformations, the sequential adsorption processes can be monitored by measuring crystal structures at different temperatures and/or gas pressures. For large-pore PCPs with weak gas affinity, this can be done by variable-temperature measurement with a crystal sealed with the targeted gas in a glass capillary, during which the temperature and pressure are simultaneously changed, but the gas amount in the capillary

(including the crystal) is constant. Although the precise pressure is unknown at each measurement temperature, this simple method can give information somewhat similar to the gas sorption isotherm/isobar. For example, single-crystal structures of $[Zn_4O(bdc)_3]$ (MOF-5) sealed in glass capillary with either Ar or N_2 illustrated eight symmetry-independent adsorption sites sequentially from 293 to 30 K.[96] For small-pore PCPs with strong gas affinity, excess gas in the capillary always lead to saturated adsorption even at high temperatures. To vary the gas loading precisely, the gas pressure must be controlled. For N_2 adsorption, the crystal may be exposed in the temperature-controlling nitrogen flow to carry out constant-pressure (1 atm) and variable-temperature measurements, which reflect the isobars and similar to the isotherms. More commonly, the gas pressures are roughly controlled by sealing the crystal at different conditions, in which the exact gas pressure is unknown for the measurement. Precise control of gas pressure can be achieved by connecting the sample tube with a gas-dosing manifold, which has been widely utilized in PXRD,[93, 97-99] but rarely used in SCXRD.[100]

To overwhelm the serious thermal motion and disorder of gas molecules, crystal structures of gas-loaded PCPs are usually measured at temperatures as low as possible at the saturated adsorption state. In general, even at the just-mentioned optimum states, determination/refinement of a gas-loaded crystal structure is still very difficult, in which restraints/constraints on molecular geometries and/or thermal parameters are usually necessary.[101, 102] Depending on the measurement method and condition, sample quality and nature, as well as the type of gas, the obtained crystal structures vary a lot in quality and can provide very different amount of structural information. Compared with PXRD,[92, 103] the high-resolution of SCXRD are particularly beneficial for determination of gas-loaded crystal structures, in which the precise adsorption site, orientation, and thermal motion of gas molecules, as well as the small structural alternation of the host framework can be obtained. In exceptional cases, usually for high boiling-point gases such as CO_2, high-quality SCXRD data and strong adsorption/confinement can be obtained to reveal the thermal motion of gas molecules, even at room temperature.[104, 105] Some recent examples are discussed below.
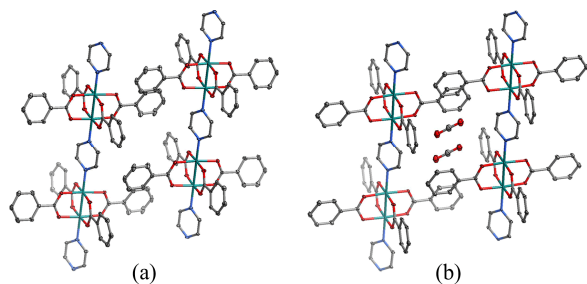
Fig. 18 The single-crystal structures of (a) $[Rh_2(bza)_4(pyz)]$ and (b) CO_2-included $[Rh_2(bza)_4(pyz)]$ measured at 90 K. Thermal ellipsoids are drawn at 30% probabilities. Hydrogen atoms are omitted for clarity.

Takamizawa *et al.* used SCXRD to study the adsorption behaviours of a variety of gases in flexible PCPs $[M^{II}_2(bza)_4(Rpyz)]$ (M = Cu, Rh; Hbza = benzoic acid; Rpyz = pyrazine derivatives) consisting of parallelly packed 1D chains and isolated cavities.[106] For example, $[Rh_2(bza)_4(pyz)]$ showed a typical two-step CO_2 isotherm at 195 K and a high CO_2

adsorption enthalpy of 43 kJ mol^{-1} at zero coverage.[107, 108] A CO_2-saturated single-crystal structure was measured at 90 K, which adopted the triclinic space group P-1. On the other hand, the guest-free crystal was monoclinic ($C2/c$ at 90 K and $C2/m$ and 298 K, T_c = 200 K). After adsorption of CO_2, the void volume increased from 16.2% to 20.2%. Based on the single-crystal structures, the framework expansion and distortion were explained by expansion of the interchain distances, slipping of neighbouring chains, and tilting of the π···π stacked phenyl rings of bza$^-$ ligands (Fig. 18). The adsorbed CO_2 molecules were tightly confined in the channel and interact with the phenyl rings on the pore surface *via* phenyl···CO_2-quadrupole interaction. Using the same sealed single-crystal, *in-situ* variable-temperature SCXRD analyses revealed that all the crystal structures adopted the triclinic space group P-1, and the CO_2 uptake gradually decreased with the increased temperature as observed in the variable-temperature adsorption isotherms.[109] Variable-temperature ^2H NMR spectroscopy for $[Rh_2(bza-d5)_4(pyz)]$ in a constant CO_2 pressure (0.1 Mpa) showed that temporary rotations of the ligand phenyl rings were responsible for CO_2 diffusion between the isolated cavities.[107] Such thermodynamically unstable states can be hardly visualized by crystallography directly. Similar monoclinic to triclinic phase transitions were also observed for N_2, NO, CH_4, O_2, and SO_2, which exhibited two-step (N_2), S-shaped (CH_4), or typical Langmuir (NO and O_2) isotherm.[110-112] On the other hand, the NO_2-loaded crystal maintained the original group space $C2/c$ and the adsorbed NO_2 molecules existed as N_2O_4.[110] The phase transition and structural transformation of $[M_2(bza)_4(Rpyz)]$ can be altered by ligand substitution.[107, 113] For example, due to the steric hindrance from the methyl groups, the 1D chain of $[Rh_2(bza)_4(Mpyz)]$ switches from zigzag to straight before and after CO_2 adsorption.[113]

Takamizawa *et al.* also observed the precise location of H_2 molecules in $[Rh_2(bza)_4(pyz)]$ using in-house SCXRD.[114] The H_2 adsorption isotherm (77 K) for $[Rh_2(bza)_4(pyz)]$ showed two obvious steps, indicating similar structure transformation as for other much heavier gases.[107, 109] Single crystal of $[Rh_2(bza)_4(pyz)]$ was sealed in a glass capillary with H_2 at 77 K and 1 atm, and subjected to SCXRD measurement at 90 K, which retained the original space group $C2/c$ with a unit-cell volume (3258 Å^3) slightly larger than that of the guest-free form at 93 K (3244 Å^3). Two H_2 molecules parallel to each other were strongly confined in the small cavity, forming close contacts with the benzoate edges (H···O = 2.57–2.91 Å). The number of hydrogen molecules observed in this crystal structure was consistent with the first-step uptake in the isotherm measured at 77 K. It could be imagined that a crystal structure corresponding to the second-step might be similar to those of the heavier gases, but neither 77 K nor much higher H_2 pressure can be achieved by common means. An example of H_2-induced framework distortion accompanying crystal-symmetry change was observed by Wright *et al.* in a 3D PCP $[Sc_2(bdc)_3]$ by using synchrotron SCXRD at 80 K.[100] However, the location of the seriously disordered H_2 could not be determined unambiguously. It should be also noted that, due to the very weak scattering factor of proton for X-ray radiation, neutron diffraction using D_2 as the guest are generally necessary to obtain the location of H_2 molecules in porous crystals.[115]

We used the unique framework flexibility and pore surface structure of MAF-2 to store C_2H_2 and separate it from CO_2, which showed S-shape isotherms near room temperature,

suggesting framework distortion and/or guest-guest interaction around the inflection points.[104] Compared with normal Langmuir-type isotherms, the S-shape isotherm is more beneficial for gas storage and separation, because it exhibits not only high uptake at high pressure but also lower residue at low pressure. Therefore, MAF-2 can store 40 times more C_2H_2 than an empty cylinder at the normal working condition (1.0-1.5 atm for safety reason). Also, MAF-2 exhibited a very high C_2H_2/CO_2 uptake ratio of 3.7 at 298 K and 1 atm, although their adsorption enthalpies differed only by 4.0-6.7 kJ mol^{-1}.[95] Single-crystal structures of the guest-free, C_2H_2- and CO_2-saturated MAF-2 were measured at 123 K. The unit-cell parameters of the C_2H_2- and CO_2-saturated phases are 1.0% and 0.6% smaller than that of guest-free MAF-2, confirming the role of framework flexibility and stronger binding for C_2H_2. The C_2H_2 molecule can be refined anisotropically without any restraint, giving a very precise C–C bond distance of 1.146(9) Å. Similar high-quality single-crystal structures were also obtained even at 293 K, indicating the strong fixation of C_2H_2. In contrast, soft restraints on the C=O bond lengths of CO_2 were necessary, and the anisotropic refinement could not be applied at higher temperatures. More interestingly, C_2H_2 and CO_2 locate completely different in MAF-2. The molecular long axis of C_2H_2 points to the planar $Cu_2(Rtz)_2$ fragment of the host framework, forming weak C-H···N interactions with the coordinated N atoms (C···N 3.44 and 3.47 Å), and six C_2H_2 molecules form a chair-like supramolecular hexamer with weak C-H···C contacts (C···C 3.69 Å) (Fig. 19). On the other hand, CO_2 lies on the $Cu_2(Rtz)_2$ planar fragment, forming close contact with the coordinated N atoms (C···N 3.40 and 3.41 Å) and surrounded by many ethyl groups, and six CO_2 molecules form a distorted octahedral arrangement with relatively long intermolecular contacts (C···O 4.58 Å). A series of single-crystal structures with different C_2H_2 and CO_2 loadings were also measured at 195 K, which showed that the framework distortion starts at very low loading and almost finished at 20% loading, and the thermal motion of the host framework decreases with increased loading, being consistent with the energetic trends observed in the gas isotherms. These results demonstrated that in large pores, C_2H_2 and CO_2 with reversed quadruple moments can find their right way to interact with the polar pore surface, even with coordinated azolate N atoms as the most electronegative points. Also, very small framework distortions can effectively change the isotherm shape and relative storage/separation properties.

Fig. 19 Single-crystal structures of MAF-2·C_2H_2 and MAF-2·CO_2 measured at 123 K. (a-b) The local host-guest structures shown in space-filling mode with gas molecules also drawn with thermal ellipsoids (probability 30%). (c-d) The chair-like of C_2H_2 hexamer and distorted octahedral CO_2 hexamer (dashed lines represent the shortest intermolecular separations, C···H 2.80 Å and C···O 4.58 Å).

Using uncoordinated azolate N-donors, CO_2 can be strongly fixed in the crystal through supramolecular interactions. Recently, we reported a flexible PCP [$Zn_2(btm)_2$]·$4H_2O$ (MAF-23·$4H_2O$, H_2btm = bis(5-methyl-1H-1,2,4-triazol-3-yl)methane) functionalized with pairs of uncoordinated triazolate N-donors serving as guest-chelating claws.[116] MAF-23 showed very high CO_2 adsorption enthalpy of 47.4±1.3 kJ mol^{-1} at near-zero coverage and CO_2/N_2 selectivity of 82 at 298 K, as well as an unexpectedly high saturation CO_2 uptake (3.0 and 2.0 CO_2 per formula unit for observed and predicted values, respectively). Single-crystal structures of MAF-23·xCO_2 (x = 0.00, 0.07, 1.5, 2.8) were successfully measured at 195 K (Fig. 20). The x values were determined by free refinements. Measurement of the single-crystal structure of MAF-23·$3CO_2$ was failed because the crystals saturated with CO_2 cracked easily, indicating that the crystals expanded enormously at the saturated adsorption state. At near zero loading, *i.e.*, MAF-23·$0.07CO_2$, a CO_2 molecule was chelated by one of the two crystallographically independent guest-chelating claws, which possessed a methyl group at the ortho position of the N-donor, demonstrating the weak electron donating effect of the methyl group. Further, there were very short intermolecular N···C separations (2.90(4)-3.00(4) Å), being consistent with the high near-zero-coverage CO_2 adsorption enthalpy derived from the sorption isotherms. When the CO_2 uptake increased, the unit-cell volume of MAF-23 continuously increases due to the distortion of coordination geometries of the Zn(II) ions and ligand shapes around the methylene groups, which explained the excess CO_2 uptake. Also, two crystallographically different molecular claws in MAF-23 deform in opposite directions with increased CO_2 uptake, which were interpreted by the convergent attraction and steric repulsion of CO_2 molecules. At moderate and high loadings, the chelated CO_2 molecules in MAF-23·$1.5CO_2$ and MAF-23·$2.8CO_2$ can be anisotropically refined without any restriction even at 298 K, indicating the exceptionally strong binding affinity of the guest-chelating claws.

(a)

(b)

(c)

(d)

(a)

(b)

(c)

(d)
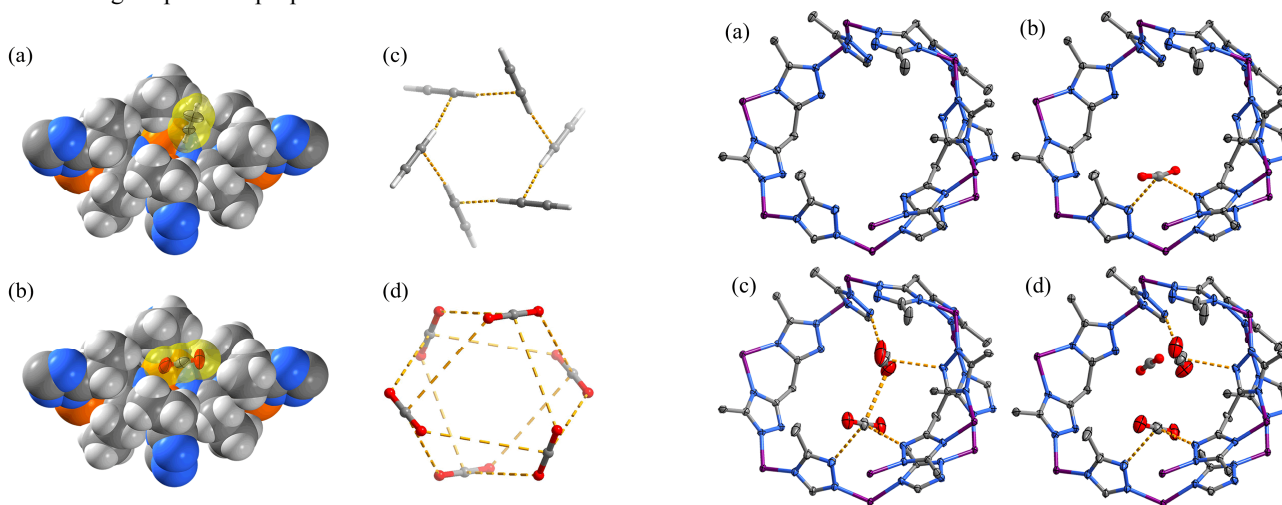
Fig. 20 Single-crystal structures of MAF-23·xCO_2 measured at 195 K. (a-d) x = 0.00, 0.07, 1.5, and 2.8, respectively. Hydrogen atoms are omitted for clarity. Thermal ellipsoids (probability 30%) are drawn for atoms refined anisotropically, while other atoms are drawn in the ball-and-stick mode. Short intermolecular contacts are shown as dashed bonds.

Gas adsorption isotherms showing gate-opening or multistep features are generally induced by significant structural transformation of the host framework. For example, Kitagawa *et al.* observed CO_2-induced cleavage and generation of coordination bonds in a flexible PCP [Cu(pydc)(bpp)] (H_2pydc = pyridine-2,3-dicarboxylic acid; bpp = 1,3-bis(4-pyridyl)-propane) possessing a 2D bilayer structure.[117] The CO_2 isotherm at 195 K showed a gate-opening increase at P/P_0 = 0.23, which was confirmed by SCXRD at the same temperature. Single-crystal structures of guest-free and CO_2-saturated [Cu(pydc)(bpp)] were measured at 373 and 193 K, which adopted the space groups $Pca2_1$ and $Pbcn$, and unit-cell volumes of 3843(2) and 4312(5) $Å^3$, respectively. The CO_2 adsorption induced the formation of a Cu-pyridyl bond (Cu–N changed from 10.38 to 2.28 Å), which doubled the numbers of pillars between the two layers, and expanded the thickness of the bilayer from 11.9 to 14.0 Å. There were two independent CO_2 molecules, one of which located between two adjacent bilayers while another located inside the internal channel of the bilayer that was originally occupied by the pendant pyridyl groups. Surprisingly, the CO_2 molecules interact with the carboxylate O atom (C···O 2.90–3.05 Å) and edges of phenyl rings (O···C 3.36–3.49 Å) on the pore surface, rather than the uncoordinated pyridyl nitrogen atoms or the unsaturated Cu(II) ions (presented in the guest-free state). One of the two independent CO_2 molecules was refined anisotropically, indicating strong host-guest interactions. Detailed analysis of the crystal structure shows that this CO_2 molecule is chelated by a pair of uncoordinated carboxylate oxygen atoms from two carboxylate groups (C···O 2.90-3.04 Å). One of these two uncoordinated oxygen atoms (Cu···O 2.92 Å) was displaced from its weakly ligated Cu(II) ion in the guest-free phase (Cu–O 2.63 Å). In contrast, another CO_2 interacts only with a coordinated carboxylate oxygen atom (C···O 3.05 Å) (Fig. 21). Actually, this CO_2-induced structural transformation was first observed during activation of the as-synthesized compound [Cu(pydc)(bpp)]·$5H_2O$, meaning that CO_2 gas can play the same role as high boiling-point liquid H_2O.
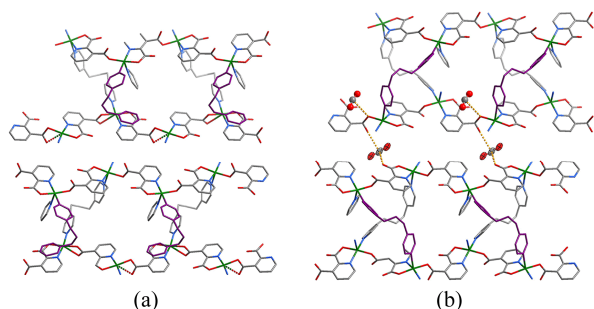
purple). Thermal ellipsoids (probability 30%) are drawn for CO_2 molecules refined anisotropically, while other CO_2 molecules are drawn in the ball-and-stick mode.

Solvent-induced framework distortion also inspired the elucidation of abnormal N_2 adsorption behaviour for SOD-[Zn(mim)$_2$] (MAF-4,[118, 119] also known as ZIF-8,[120] Hmim = 2-methylimidazole), which is very thermally and chemically stable and was considered to be a very rigid framework. Two-step N_2 adsorption isotherms are generally observed for MAF-4, which was previously explained as guest rearrangement.[120] Nevertheless, the pore volume calculated from its crystal structure (0.54 cm^3 g^{-1}), using the SOLV routine in Platon,[121] is consistent with the first-step pore volume (0.55 cm^3 g^{-1}) rather than the second-step (0.67 cm^3 g^{-1}) of the N_2 isotherms. Moggach *et al.* found that MAF-4 can distort to open the 4-membered ring apertures at extremely high pressure using methanol/ethanol mixture as a hydrostatic medium, although the solvent molecules were completely disordered.[122] Later, Fairen-Jimenez *et al.* successfully used the high-pressure structure of MAF-4 to explain the two-step N_2 isotherms by computer simulation and further confirmed by using synchrotron PXRD.[123] The N_2 molecules in the synchrotron PXRD structure of N_2@MAF-4 were highly disordered. For example, in the centrosymmetric 4-membered ring channel which can only adopt one N_2 molecule, there were two disordered N_2 molecules resided at the two ends.
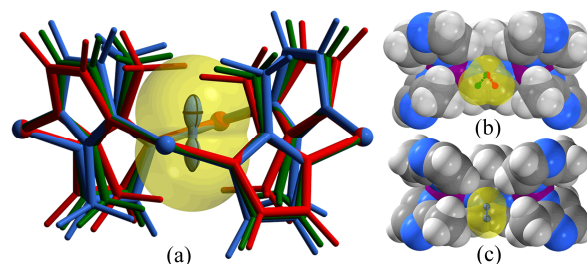
Fig. 22 Comparison of the temperature-dependent host-guest structures of a MAF-4 single-crystal in N_2 flow. (a) The 4-membered ring apertures (red, green, and blue for 113, 111, and 109 K, respectively). The N_2 molecule at 111 K is omitted for clarity. (b) The primary adsorption site at 113 K (left, the two possible locations of the disordered N_2 molecule are shown in red and green, respectively) and 109 K (right). Thermal ellipsoids (probability 30%) are drawn for N_2 molecules refined anisotropically. The van der Waals surfaces of the N_2 molecules are also shown to highlight their compatibilities with the pore surfaces.

We measured a series of variable-temperature single-crystal structures for MAF-4 under open nitrogen flow by using an in-house X-ray diffractometer (Fig. 22).[124] The expected phase transition was observed at 113-108 K, below which the imidazolate ligands tilted to open the 4-membered ring. Importantly, the N_2 molecules in the low-temperature phase were highly ordered. Especially, inside the small 4-membered ring channel, an N_2 molecule located exactly at the centre. The centrosymmetric nature of this N_2 molecule was confirmed by *in-situ* variable-temperature Raman spectra under identical experimental conditions. Below the phase transition temperature, the characteristic Raman peak of N_2 increase significantly, although the N_2 inside the 4-membered ring aperture only constitute a small portion of the total adsorption

Fig. 21 (a) Single-crystal structures of [Cu(pyrdc)(bpp)] measured at 373 K and (b) CO_2-included [Cu(pyrdc)(bpp)] measured at 195 K. Hydrogen atoms are omitted for clarity. The. The host frameworks are drawn in the stick mode (hydrogen atoms are omitted for clarity, and the bpp ligands underwent significant conformation change are highlighted in

amount. An intermediate phase with partially opened 4-membered rings was measured at 111 K, which was explained as a solid-solution structure of the fully closed and fully opened phases. Similar phase transition and N_2 locations were also observed for $[Zn(mtz)_2]$ (MAF-7, Hmtz = 3-methyl-1,2,4-triazole) with more polar pore surface and higher guest affinity, which showed a phase transition at 117-115 K, being *ca.* 4-7 K higher than that of MAF-4. Due to the sharp phase transition, the intermediate phase of N_2@MAF-7 was obtained by a kinetic SCXRD method (time-dependent) instead of the thermodynamic SCXRD method (temperature-dependent) as used for N_2@MAF-4. These results demonstrated the notable precision and versatility of SCXRD.

A much larger gas-induced framework breathing was observed by Omary *et al.*, who noticed that the two-step N_2 and O_2 adsorption isotherms for $[Ag_6(ftz)_6]$ (FMOF-1, Hftz = 3,5-bis(trifluoromethyl)-1,2,4-triazole) implied two pore-filling sequences.[125, 126] A series single-crystal structures of FMOF-1 exposed in N_2 at atmosphere pressure were determined at 295-90 K. The temperature-dependent unit-cell parameter profiles exhibited two sections, being coincident with the two-step N_2 adsorption isotherm. During temperature decrease, the unit-cell volume first gradually decreased from 7462 $Å^3$ at 295 K to 6824 $Å^3$ at 119 K, and then suddenly increases to 7719 $Å^3$ at 90 K, corresponding to a large framework expansion. Six adsorption sites were assigned based on the appearance sequence during temperature decrease. N_2 molecules appeared sequentially from 150 to 119 K, at the first three adsorption sites at different positions of the channel, which attracted the channel surface to shrink the crystal. When the measurement temperature further decreased below 119 K, N_2 molecules appeared at the other three adsorption sites inside the originally very small cavities, which expand the cavities and channels, as well as the whole crystal due to steric hindrance effects (Fig. 23). Considering that the pore sizes in the expanded phase are still extremely small, solvent molecules with much larger molecular sizes may not be able to enter these pores, at mild conditions, to induce such a large framework expansion.[122]
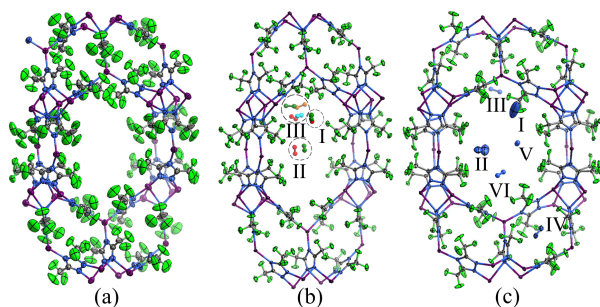
Fig. 23 (a-c) Single-crystal structures for FMOF-1 under nitrogen atmosphere measured at 295, 119 and 90 K, respectively. Thermal ellipsoids (probability 30%) are drawn for atoms refined anisotropically, while other atoms are drawn in the ball-and-stick mode. The possible locations of each disordered N_2 molecules are shown in different colours.

Obviously, depending on the framework flexibility of the PCP and the change of species/amount of the guest molecules, the magnitude of guest-induced structural transformation can vary significantly. Although small structural transformations have been less focused, SCXRD has revealed interesting host-guest and guest-guest structures in such systems. It should be

noted that, to precisely compare the crystal structures with different guest-loadings, they should be ideally measured at the same temperature to avoid the thermal expansion effect (see Section 5).

4. Structural transformation induced by post-synthetic modification

Although PCPs are less robust than conventional adsorbents, many of them can undergo post-synthetic modification (PSM) by means of covalent reaction on the organic ligands, metal/ligand exchange, capture, and release, and many other means.[127-131] The similarity of PXRD patterns between the original and modified samples is usually used as an evidence for retention of framework connectivity, because most PSM examples produce isostructural compounds. Compared to adsorption/desorption of guest molecules, the harsh action of PSM generally produce more damage on the sample crystallinity and single-crystallinity. So far, some SCXRD data have been reported for PCPs after PSM, which not only indicate the robustness of the crystal and exclude recrystallization during solution-based reaction, but also reveal some structural detail of the modified materials. On the other hand, because the changed components in the PCP crystals are usually disordered and/or non-periodic, even SCXRD can hardly determine the modification degrees (usually much lower than 100%) accurately.

4.1 Covalent modifications

Solid-state photochemical [2+2] cycloaddition within crystals is a unique solvent-free way to synthesize regio- and stereo-specific, highly strained cyclobutane derivatives. Owing to the absence of guest diffusion, the sample single-crystallinity can be usually retained,[132-137] but porosity has been rarely demonstrated for these compounds.[137] PCP crystals can be covalently modified by condensation of reactive moieties on the pore surface with guest reactants, decomposition of thermal/light sensitive functional groups, and other types of organic reactions.[127] While most of these reactions/products are characterized by NMR, mass spectroscopy and PXRD, some single-crystal structures of the modified PCP crystals have been reported.[138-145] However, most SCXRD data suffer from symmetry-induced disorder, thermal motion of side groups in the large cavities, relatively low conversion degree, and/or degraded single-crystallinity. Only in a couple of examples, SCXRD revealed the structures of the obtained functional group and/or the reaction progress.[145, 146]

Kitagawa *et al.* utilized an photolysis reaction to produce highly reactive aryl nitrene in a flexible PCP $[Zn_2(aipa)_2(bpy)_2]\cdot1.5DMF$ (H_2aipa = 5-azidoisophthalic acid, CID-N$_3$).[145] *In-situ* synchrotron SCXRD measurements under an ultrahigh-pressure Hg lamp were carried out. During the photoirradiation process, the space group of the crystal was gradually transformed from $P2/n$ to $C2/m$. Comparison of the crystal structures obtained before and after photoirradiation demonstrated the photolysis of the azide groups and generation of nitrene groups, although the latter of which showed disorder in three positions (Fig. 24). The unstable nitrene groups in the modified crystal can react with O_2 molecules to generate nitro and nitroso groups. Similarly, Cohen *et al.* introduced hydroxy groups onto the pore surfaces of two isostructural PCPs via photolysis of the nitrobenzyl protecting groups.[146] SCXRD

showed that the resultant framework remained intact but the protecting group nitrobenzyl disappeared.
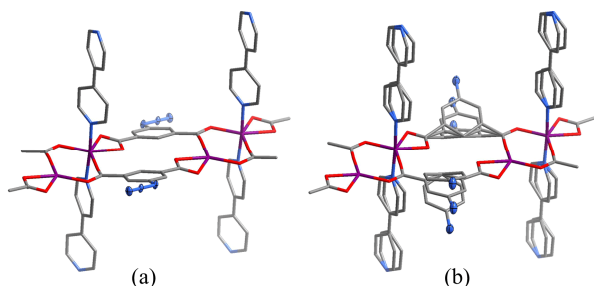
Fig. 24 The single-crystal structures of (a) $[Zn_2(aipa)_2(bpy)_2]$ measured at 93 K and (b) $[Zn_2(nipa)_2(bpy)_2]$ (H_2nipa = 5-nitreneisophthalic acid) measured at 77 K. Thermal ellipsoids (probability 30%) are drawn for the azido and nitrene groups, while other atoms are drawn in the stick mode. Hydrogen atoms are omitted for clarity.

4.2 Coordination modifications

Some PCP crystals can undergo coordination modification to give isostructural materials that may not be accessible by direct self-assembly and crystallization.[147-154] Here, coordination modification refers to exchange and capture/release of metal/ligand ions on the coordination framework (Fig. 25). Exchange of counter ions within the channels of charged host frameworks is a well-known phenomenon. However, due to the reversibility of coordination bonds, whether the ion exchange processes in PCPs undergo the solvent-assisted SCSC transformation or recrystallization is usually controversial. In recent years, the reactivity of PCP crystals with ionic compounds is emerging as a powerful tool for modification of the host framework structures. Regardless of the reaction mechanism (either SCSC transformation or recrystallization), SCXRD is the key method for characterization of the modified materials.
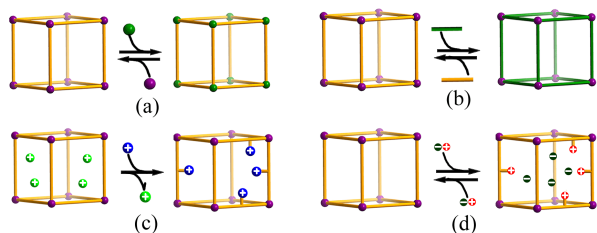
Fig. 25 Cordination modifications of the host framework in different ways. (a) Exchange of cations on the coordination framework. (b) Exchange of anionic ligand on the coordination framework. (c) Exchange of counter ion by the coordinated metal ion. (d) Release/capture of ionic compounds.

4.2.1 Exchange of metal/ligand ions
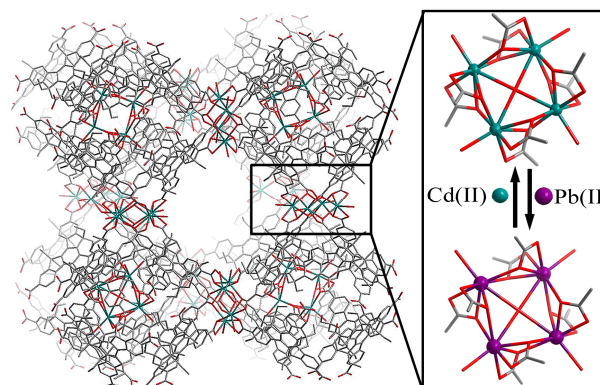
Fig. 26 Post-synthetic metal ion exchange between isostructural frameworks $[(Cd_4O)_3(hett)_8]$ and $[(Pb_4O)_3(hett)_8]$. Hydrogen atoms are omitted for clarity.

As a part of the host coordination framework, the metal ion is cooperatively coordinated by multiple ligands, which is expected to be difficult to undergo ion exchange except that on the defects and/or outer crystal surfaces. Nevertheless, not only the counter ion but also the framework metal ion can be exchanged by other metal ions.[155, 156] For example, Kim et al. reported that the metal ions in the PCP $Cd_{1.5}(H_3O)_3[(Cd_4O)_3(hett)_8]\cdot6H_2O$ (H_3hett = ethyl substituted truxene tricarboxylic acid) could be completely exchanged by Pb(II) in the SCSC manner, and the process was reversible (Fig. 26).[157] SCXRD analyses revealed that the crystal before and after metal-node exchanged have similar unit-cell parameters but significantly different coordination bond lengths. During the exchange process, little change in the shape, size, or appearance (except some colouring) were observed for a single crystal from a series of optical microscope images, and the preservation of bulk crystallinity was confirmed by in-situ PXRD. Increase of the Pb(II) occupancy and decrease of the Cd(II) were directly revealed by time-dependent in-situ SCXRD. Nevertheless, the Pb/Cd ratios in the modified crystals were determined by ICP-atomic emission spectroscopy.

Similar to the metal ion, the organic bridging ligand within the host framework might be exchanged by other similar ligands, which is useful to modify the pore surface and pore size of the crystal. For example, Hupp et al. demonstrated that the linkers in highly stable zeolitic PCPs including MAF-4[158] and RHO-[Cd(eim)$_2$] (CdIF-4, Heim = 2-ethylimidazole)[159] can be substituted by other imidazolate ligands in the SCSC fashion, giving isostructural zeolitic frameworks unavailable by direct synthesis. NMR spectroscopy showed that the ligand exchange process was reversible and the exchange percentages can be up to 85% and 100%, respectively, being coincident with the occupancies of the substituent group of imidazolate ligands obtained by SCXRD. More surprisingly, Rosi et al. exchanged the dicarboxylate ligand in $(Me_2NH_2)_4[Zn_8O_2(ad)_4(ndc)_6]\cdot4DMF\cdot31H_2O$ (bio-MOF-100, Had = adenine, H_2ndc = 2,6-naphthalenedicarboxylic acid) by longer dicarboxylates to give isoreticular single crystals with drastically increased void volumes.[160] The SCSC transformation processes were proved by a series of optical images of a single crystal at different immersion times.
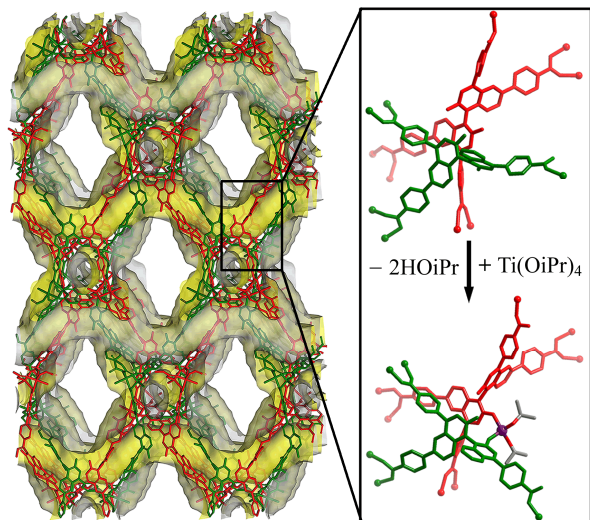
Fig. 27 Post-synthetic conversion from $[Zn_2(H_2dhbtc)]$ to $[Zn_2(Hdhbtc)Ti_{0.5}(OiPr)(H_2O)]$. Hydrogen atoms are omitted for clarity.

External metal ions can also exchange the acidic proton on the coordination framework. For example, Cohen *et al*. showed that the 2-phenylpyridine groups in some PCP crystals consisting of 2-phenylpyridine-5,4'-dicarboxylate ligands can react with $[Ir^I(cyclooctadiene)(OCH_3)]_2$ or $[Rh^I(cyclooctadiene)Cl]_2$ to give cyclometalated Ir and Rh complexes.[161] SCXRD structural analysis confirmed that the Ir(I) or Rh(I) were chelated by one pyridine nitrogen atom and one carbanion atom from the same dcppy^{3-} ligand. ICP-MS showed that the frameworks contained Ir or Rh ranging from 0.6 wt% up to 8.3 wt%. Lin *et al*. showed that the free phenolic hydroxyl groups in single crystals of $[Zn_2(H_2dhbtc)(DMF)(H_2O)]\cdot 2EtOH\cdot 4.3DMF\cdot 4H_2O$ (H_6dhbtc = (R)-2,2'-dihydroxy-1,1'-binaphthyl-4,4',6,6'-tetracarboxylic acid) can react with a toluene solution of $Ti(OiPr)_4$ (HOiPr = isopropanol) to give $[Zn_2(Hdhbtc)Ti_{0.5}(OiPr)(H_2O)]$.[162] SCXRD structural analysis of the modified crystal revealed that the Ti(IV) ion was coordinated by two deprotonated binaphthol hydroxyl groups from the two independent coordination networks and two original OiPr$^-$ groups in a normal tetrahedral configuration. As a result, the host framework transformed from 2-fold interpenetrated 3D networks to a non-interpenetrated 3D network (Fig. 27).

Exchanging counter ions by ions with coordination abilities can also achieve coordination modification of PCPs. For example, Schröder *et al*. immersed $(H_2ppz)[In_2(qptc)_2]\cdot 3.5DMF\cdot 5H_2O$ (NOTT-200, ppz = piperazine; H_4qptc = 1,1',4,1'',4,1'''-quaterphenyl-3,5,3''',5'''-tetracarboxylic acid) in a saturated solution of LiCl in water/acetone (1:1 *v/v*) at room temperature for ten days to give $[Li_{1.5}(H_3O)_{0.5}In_2(qptc)_2]\cdot 11H_2O$ (NOTT-201), during which the sample retained single-crystallinity (Fig. 28).[163] In NOTT-201, the Li/In molar ratio was determined by ICP-MS to be 0.75. SCXRD analysis showed that NOTT-201 has the same topology of NOTT-200 and all the H_2ppz^{2+} cations have been replaced by Li(I) and protons. The Li(I) ion was tetrahedrally coordinated by two H_2O molecules and two carboxylate oxygen atoms. After exchange of the large guest H_2ppz^{2+}, the pore size was increased from 4.3 Å of NOTT-200 to 8.3 Å of NOTT-201. Activation of NOTT-201 can remove the coordinated and

lattice H_2O molecules. Although the coordinated environment of the Li(I) ions in the activated samples was not directly measured, the isosteric heat of H_2 adsorption for activated NOTT-201 is higher than that of activated NOTT-200, indicating the strong interaction between H_2 and coordinatively unsaturated Li(I).
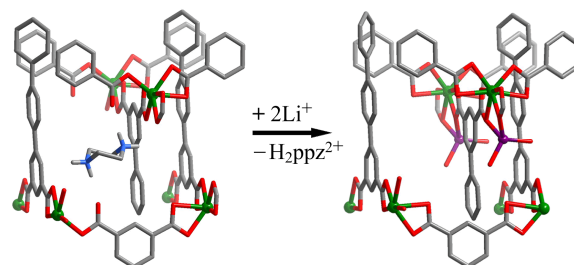
Fig. 28 Post-synthetic conversion from NOTT-200 to NOTT-201. Except for protonated sites of ppz, hydrogen atoms are omitted for clarity.

4.2.2 Capture/release of metal ions

Besides ion exchange, external metal ion can be also introduced onto the host network of PCP crystals, during which the counter anion also enter the pores. Zaworotko *et al*. reported a series of PCPs $[CdCl(tmpp)][M_xCl_yCd_4(bpt)_4(solvent)_z]$ (H_2tmpp^{4+} = *meso*-tetrakis(4-N-methylpyridyl)porphine; H_3bpt = bi-phenyl-3,4',5-tricarboxylic acid; M = Na$^+$, Ba^{2+}, Mn^{2+}, Cd^{2+}; x = 1, 0.5, 0.5, 1; y = 0, 0, 0, 1; z = 3, 3, 2, 3; respectively) obtained by soaking single crystals of $[Cd(tmpp)(solvent)][Cd_4(bpt)_4]$ in MeOH solutions of metal chloride salts.[164] SCXRD structural analyses revealed that the introduced ions were coordinated by the carboxylate oxygen atoms of the host framework and solvent molecules. Meanwhile, the introduced Cl$^-$ replaced the coordinated solvent molecules of the cationic Cd(II)-porphyrinate guest (Fig. 29). Interestingly, crystallographic refinement and solution-state UV/Vis spectroscopy showed that there was no exchange to the Cd(II) of both the anionic host network and the cationic porphyrinate guest.
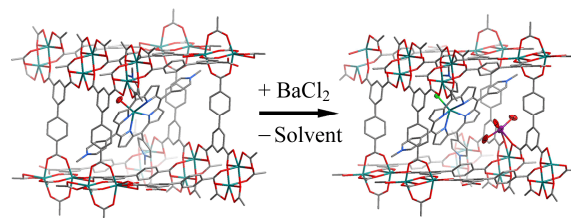
Fig. 29 Post-synthetic conversion from $[Cd(tmpp)(solvent)][Cd_4(bpt)_4]$ to $[CdCl(tmpp)][Ba_{0.5}ClCd_4(bpt)_4(solvent)_3]$. Thermal ellipsoids (probability 30%) are drawn to highlight atoms involved in the exchange, while other atoms are drawn in the stick mode. Hydrogen atoms are omitted for clarity.

Neutral coordination framework can also capture external metal ions. For example, Hardie *et al*. reported a self-entangled 3D uninodal 4-connected network $[Zn(ipa)(bpbpdc)]\cdot 2DMF$ (bpbpdc = N,N'-bis(pyridin-4-yl)-2,2'-bipyridine-5,5'-

dicarboxamide) consisting of a very long 4,4'-bipyridyl-type linker with a 2,2'-bipyridyl backbone.[165] Interestingly, the 2,2'-bipyridyl fragments of the long bpbpdc ligands were uncoordinated, and each pair of 2,2'-bipyridyl fragments are placed closely in a cross configuration suitable for metal chelating. Soaking the pale-yellow as-synthesized crystals in a DMF solution of $CuCl_2$ for 3 weeks gave yellow-brown crystals of $[ZnCu_{1/3}(ipa)(bpbpdc)]Cl_{1/3}\cdot[CuCl_2]_{0.3}\cdot n$DMF (2/3 of the free chelating sites were occupied by Cu), whose structure and chemical formula were determined by synchrotron SCXRD and energy-dispersive X-ray (EDX) spectroscopy. In the modified crystal, the Cu ion was tetrahedrally coordinated by two 2,2'-bipyridyl moieties from two independent ligands with Cu–N distance 2.066(5) Å, indicating a +1 oxidation state (Fig. 30). Obviously, this structural transformation was facilitated by the strong Cu(I) affinity of a pair of cross-placed 2,2'-bipyridyl fragments. In this redox process, the solvent DMF was assigned as the reductant. Due to the additional tetrahedral Cu(I) nodes, the coordination network was partially converted into a binodal 4-connected network.
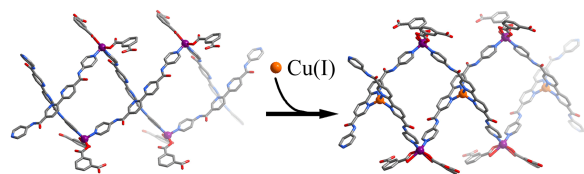
Fig. 30 Post-synthetic conversion from [Zn(ipa)(bpbpdc)] to $[ZnCu_{1/3}(ipa)(bpbpdc)]Cl_{1/3}\cdot[CuCl_2]_{0.3}$. Hydrogen atoms, counter anions, and guest molecules are omitted for clarity.

Besides capture of metal ion or metal salt, the host framework can also release its ionic metal/ligand by extraction. For example, Long *et al.* showed that the embedded chloride anion in a PCP consisting of $Cu_4(\mu_4\text{-Cl})(Rta)_8$ (Rta^- = tetrazolate or 1,2,3-triazolate group) clusters can be partially extracted along with extraframework Cu(II) cations by immersing the crystal in hot CH_3OH for five days.[166] SCXRD structural analysis revealed that the Cl^- at the central position within the $Cu_4(\mu_4\text{-Cl})(Rta)_8$ unit was reduced *ca.* 50% and the lengths of the Cu-N bonds and trans Cu···Cu distances were shortened from 2.036(3) and 5.078(2) Å to 1.985(3) and 4.932(2) Å, respectively.

5. Structural transformations induced by physical stimuli

Chemical changes of the crystals, such as adsorption/desorption of guest molecules (Sections 2 and 3) and PSM (Section 4), are the commonly encountered origins for structural transformations of coordination polymers. Physical stimuli can also change the structures of coordination polymers without any alternation of their chemical compositions. Unfortunately, many of these physical stimuli-induced structural transformations only occur transiently and can be hardly studied by crystallography. Nevertheless, SCXRD has played an important role in several related fields, such as thermal expansion and spin crossover (SCO), which show small and structural alternations among different thermodynamically stable states. Similar to other properties, the host-guest chemistry of PCPs offers an additional parameter to control their framework flexibility and structural responses toward physical stimuli. To distinguish PCPs from other materials, we

only discuss examples that are controlled by inclusion of different guest molecules.

5.1 Guest-controlled thermal expansion

While thermal expansion behaviours of crystalline materials were usually studied by PXRD,[167-171] SCXRD have demonstrated advantages in observing very small structural alterations responsible for thermal expansion in coordination polymers.[172-174] For example, Kepert *et al.* found unusual isotropic negative thermal expansion (NTE) for $[Cu_2(btc)_3]$ (HKUST-1, H_3btc = 1,3,5-benzenetricarboxylic acid) with $\alpha = -4.1 \times 10^{-6}$ K^{-1} under vacuum at 100-500 K.[175] Based on a series of single-crystal structures measured at 100–500 K in 16 K steps, the NTE behaviour was elucidated by local molecular vibrations within the dinuclear $Cu_2(RCOO)_4$ paddle-wheel unit and concerted transverse vibrations of the planar linker btc^{3-}.

Since thermal expansion is sensitive to the component, connectivity, and interaction in the crystal, guest molecules can be used to modify the thermal expansion behaviour of a porous crystal. However, change of guest-loading can generally induce much larger framework distortion than for temperature, especially for flexible PCPs (see Section 2). Guest-loading is not only dependent on the species and pressure of the surrounding atmosphere. Heating a guest-containing crystal in an open condition is a general method to reduce the guest-loading. In other words, it is usually not easy to measure the pure thermal expansion property for a porous crystal in open conditions. For example, variable-temperature unit-cell parameters of FMOF-1 sealed in vacuum were measured by SCXRD, which showed very large linear positive thermal expansion (PTE) with $\alpha = +230 \times 10^{-6}$ K^{-1} and NTE with $\alpha = -170 \times 10^{-6}$ K^{-1}.[126] When the crystal was exposed in the temperature-controlling N_2 flow, the unit-cell parameters changed drastically, giving curved apparent thermal expansion profiles with inflection points at 119 K. Since the N_2 loading vary at different temperatures, it is not possible to extract the pure thermal expansion effect for the N_2-loaded crystal.

For very rigid and/or large-pore frameworks, variable guest-loading may not influence the thermal expansion behaviour of the crystal. When Yaghi *et al.* used SCXRD to study the adsorption sites for Ar and N_2 within MOF-5, they found NTE behaviour (1.2 % volume increase from 293 to 30 K, corresponding to $\alpha = -15.3 \times 10^{-6}$ K^{-1}) for the crystal sealed with N_2.[96] Later, Snurr *et al.* elucidated and further predicted the NTE behaviours of isoreticular compounds by molecular simulations,[176] and then Iversen *et al.* investigated the NTE behaviours of MOF-5 under vacuum by SCXRD at 100-500 K and synchrotron PXRD at 80-500 K, which gave $\alpha = -13.1(1) \times 10^{-6}$ K^{-1}, and the obtained structural details showed that the NTE behaviour was originated from vibrational motions (twisting, rotation, and libration) of the bridging ligand.[177]

To realize true and notable guest-controlled thermal expansion, a flexible PCP should be the first choice. Nevertheless, constant guest-loading must be ensured, which may be fulfilled by strong host-guest interactions (small channels and large/high-boiling point guests) and suitable measurement conditions (relatively low temperatures and sealed with saturated vapour of the guest to avoid guest escape). To understand the complicated host-guest interplay in the system, not only the small structural alternations of the host framework, but also the detailed host-guest and guest-guest interactions must be visualized.

Using SCXRD, Kepert *et al.* revealed the guest-dependent NTE behaviours of two nanoporous Prussian Blue analogues [ZnPt(CN)$_6$]·2H$_2$O and [CdPt(CN)$_6$]·2H$_2$O.[178] *In-situ* variable-temperature SCXRD measurements were carried out for direct comparison of the thermal expansion of the as-synthesized and guest-free crystals. While [ZnPt(CN)$_6$]·2H$_2$O (α = +1.82(15) × 10^{-6} K^{-1}) and [ZnPt(CN)$_6$] (α = -3.38(9) × 10^{-6} K^{-1}) exhibited PTE and NTE behaviours, respectively, both [CdPt(CN)$_6$]·2H$_2$O (α = -7.31(5) × 10^{-6} K^{-1}) and [CdPt(CN)$_6$] (α = -6.69(5) × 10^{-6} K^{-1}) showed similar NTE behaviours, which were elucidated by their different cavity sizes (Fig. 31a). The spherical cavities in [ZnPt(CN)$_6$] and [CdPt(CN)$_6$] were estimated to be *ca.* 45 and 65 Å^3, respectively. For comparison, an H$_2$O molecule occupies *ca.* 40 Å^3.[179] Although the H$_2$O molecules were disordered in the highly symmetric (cubic) single-crystal structures, it can be reasonable to deduce that H$_2$O forms strong interactions with the cyanide ligands on the pore surface of [ZnPt(CN)$_6$], which impedes the vibrational motion of the cyanide linkages responsible for the NTE property. For the larger-pore framework of [CdPt(CN)$_6$], such kind of host-guest interaction is much weaker or even absent, so that its NTE property is essentially independent of H$_2$O inclusion.
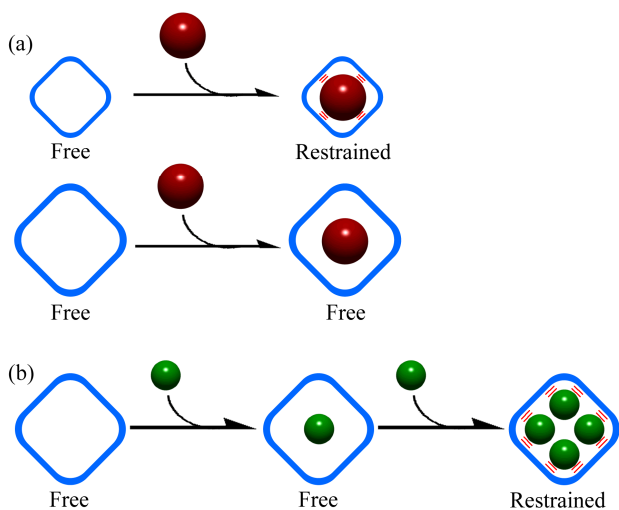
Fig. 31 Principles of the roles of (a) pore size and (b) guest quantity on framework vibration.

Kepert *et al.* reported another cubic porous framework [Cd(CN)$_2$] showing similar guest-perturbed NTE properties.[180] Crystals of [Cd(CN)$_2$]·CCl$_4$ coated with thin film of grease were subjected for SCXRD measurements, in which the temperatures were controlled by a nitrogen stream. The guest CCl$_4$ escaped above 300 K to give desolvated crystals [Cd(CN)$_2$]·*x*CCl$_4$, in which the *x* values were determined by SCXRD at 300 K. At 170–375 K, the vacant crystal [Cd(CN)$_2$] (*x* = 0) showed the largest isotropic constant NTE coefficient α = -33.5(5) × 10^{-6} K^{-1} reported so far in crystalline materials. Below 170 K, N$_2$ adsorption became un-negligible, causing apparent PTE behaviours. Such N$_2$-adsorption induced framework breathing was also observed for [Cd(CN)$_2$]·*x*CCl$_4$ with *x* = 0.64 and 0.75. On the other hand, single crystals of [Cd(CN)$_2$]·*x*CCl$_4$ with *x* = 0.64, 0.75 and 1.00 displayed smaller NTE with α = -16.9(3) × 10^{-6} K^{-1} and α = -5.7(3) × 10^{-6} K^{-1}, and even PTE with α = +10.0(2) × 10^{-6} K^{-1}, respectively. Although the CCl$_4$ guest cannot be clearly seen for symmetry-induced disorder, the guest occupancy could control the extent

of host-guest interactions and free molecular vibrations responsible for NTE (Fig. 31b).

Besides large and tunable guest-induced framework distortion, we also found interesting guest-controllable thermal expansion behaviours for the highly flexible framework MCF-18 (Fig. 32).[64] The variable-temperature unit-cell parameters of MCF-18, MCF-18·MeOH, and MCF-18·DMF were measured by SCXRD at 119-295 K. Single-crystal specimens were sealed in glass capillary under vacuum or with small amounts of corresponding solvents to ensure constant guest loading. While the shrunk framework MCF-18 showed large and constant PTE on the c-axis with α = 81 × 10^{-6} K^{-1}, the expanded frameworks MCF-18·MeOH and MCF-18·DMF displayed huge but temperature-dependent PTE on the *c*-axes with maximum coefficients α = 242 × 10^{-6} K^{-1} and 437 × 10^{-6} K^{-1}, respectively. The high porosity and flexibility, as well as the unique framework connectivity of the host framework may transform the large and isotropic thermal expansion of liquids to anisotropic or uniaxial thermal expansion on the crystals. Interestingly, when MCF-18·MeOH and MCF-18·DMF were directly put into the cold N$_2$ flow at 119 K, they possessed much smaller unit-cell volumes than those slowly cooled down from room temperature. By heating, their thermal expansion profiles gradually approached those of the slowly cooled ones. To the best of our knowledge, this "quenching" effect is similar to that from liquid water to amorphous ice, but has not been observed in other crystalline materials. The slowly-cooled and "quenched" single-crystal structures of MCF-18·DMF were measured at 119 K and compared with that measured at 295 K, which revealed some small guest relocations related to temperature change and/or cooling history. However, due to the relatively large channel size and high crystal symmetry (*R*-3*c*), the DMF molecules showed serious disorder that required strict restraints, meaning that the guest structures may not reflect their true roles reliably.
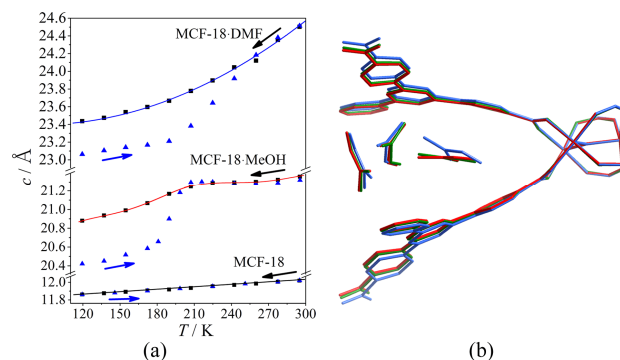
Fig. 32 (a) Temperature and history dependence of the *c*-axes of MCF-18, MCF-18·MeOH and MCF-18·DMF (arrows represent the cooling or warming directions). (b) Structural variations of MCF-18·DMF at 295 K (blue), slowly cooled to 119 K (green), and quenched to 119 K (red). Note that the guest DMF molecules in the single-crystal structures were refined with strict restraints on molecular geometry. Hydrogen atoms are omitted for clarity.

Using PCPs with very small and low-symmetry channels, the detailed host-guest interaction may be observed. For example, Barbour *et al.* reported the solvent-controlled thermal expansion in a microporous framework [Zn(OH)(niba)] (Hniba = 4-(1*H*-naphtho[2,3-*d*]imidazol-1-yl)benzoic acid), which was a pillared-rod 3D structure consisting of polymeric Zn−OH−Zn

coordination chains (Fig. 33).[181] The guest-free framework exhibited very large PTE ($\alpha_c = +127 \times 10^{-6}$ K^{-1}) and moderate NTE ($\alpha_{a/b} = -21 \times 10^{-6}$ K^{-1}) under vacuum at 100-370 K. SCXRD data of the guest-free crystal were collected at 100 K, 190 K, 270 K and 370 K, and structural detail analyses indicated that the remarkable PTE of the c-axis resulted from the increase of the Zn−OH−Zn angle with increased temperature. Interestingly, the PTE coefficient could be changed from $+76 \times 10^{-6}$ K^{-1} to $+166 \times 10^{-6}$ K^{-1} (effective at 100−295 K) by loading MeOH, EtOH, n-PrOH, and i-PrOH. The order of PTE coefficients (MeOH > EtOH > n-PrOH) can be correlated with the sizes of the guests. Single-crystal structures of the solvated crystals were measured at 100 K, which revealed that the guest molecules were located around the Zn−OH−Zn coordination chains, forming hydrogen-bonds with the adjacent uncoordinated carboxylate oxygen atoms. The smaller guests (MeOH, EtOH and n-PrOH) gave smaller Zn−OH−Zn angles compared with that of the guest-free framework, making the host framework into more "contracted" states to enhance further thermal expansion. In the case of i-PrOH inclusion, the Zn−OH−Zn angle was larger than that of the guest-free framework, indicating that the host framework was in an "expanded" state restricting the thermal expansion.
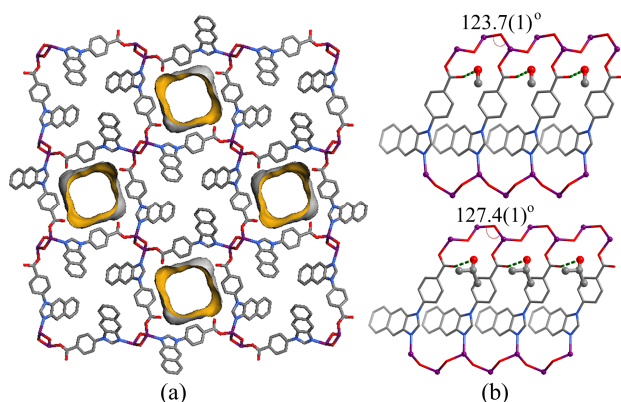
Fig. 33 (a) The host framework and pore surface structures of [Zn(OH)(niba)]. (b) The host-guest structures of MeOH- and i-PrOH-loaded [Zn(OH)(niba)] highlighting the effect of guest size.

Recently, we realized well-defined guest-controlled thermal expansion behaviour in a flexible ultramicroporous framework [Mn(34-pba)$_2$] (MCF-34, 34-Hpba = 3-(pyridin-4-yl)benzoic acid).[182] The ligand 34-Hpba with a low energy barrier for conformation change may undergo paddlewheel movement under external stimuli. The vacant framework possessing ultramicroporous channels can exclude air adsorption (N$_2$/O$_2$) even at 77 K. In addition, it is stable up to 673 K. Variable-temperature unit-cell parameters of MCF-34 were measured by SCXRD and PXRD, which exhibits constant and huge PTE ($\alpha = +224 \times 10^{-6}$ K^{-1}) and NTE ($\alpha = -107 \times 10^{-6}$ K^{-1}) over a wide temperature range (127–673 K) both in vacuum and in open-air condition (Fig. 34). Single-crystal structures of MCF-34 exposed in the temperature-controlling N$_2$ flow were measured at 127 K, 294 K and 445 K, which confirmed the remarkable thermal stability and absence of gas adsorption at low temperature. Detailed comparison of the crystal structures indicated that the large thermal expansion is attributed to the flexible and porous framework structure. The thermal expansion properties of guest-included frameworks were studied with single crystals in contact with saturated

solvent vapour sealed in a glass capillary. While other solvents gave similar thermal expansion behaviours as that of the vacant crystal, the DMF-loaded framework MCF-34·DMF underwent a phase transition at 208–215 K, accompanying a drastic crystal deformation. The thermal expansion coefficients of MCF-34·DMF above 233 K and below 208 K were larger and smaller than those of the vacant crystal, respectively, indicating the different aggregation and/or motion of guest molecules. With multiple SCXRD data collected at 127-294 K, the DMF guests were found to be highly disordered in the high-temperature phase, indicating a liquid-like structure and/or symmetry-induced disorder. On the other hand, the low-temperature phase crystal possessed a lower-symmetry space group with a doubled unit-cell volume, in which the location of DMF was well resolved, indicating that the motion of DMF molecules decreased significantly to form a solid-like structure. In the low-temperature crystal structure, a DMF molecule embedded one of its methyl groups into the pore wall, driving the conformation reversion of one-fourth ligands to generate a small pocket. This conformation reversion was transmitted to the whole crystal for a drastic deformation. Nevertheless, crystallography is not able to distinguish whether the DMF molecules are statistically disordered or dynamically moving in the high-temperature phase. Therefore, this liquid-like to solid-like rearrangement of DMF guest was further confirmed by molecular dynamic simulations and solid-state ^{2}H NMR.
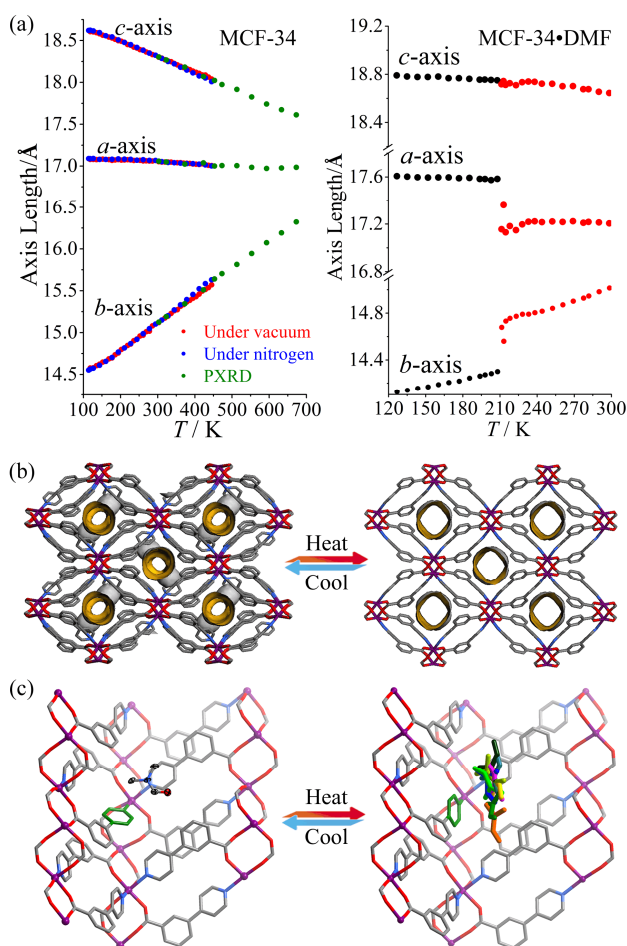
Fig. 34 (a) Temperature-dependent unit-cell parameters of MCF-34 and MCF-34·DMF. (b) The host framework and pore surface structures and (c) relocation of DMF molecules

between the low temperature (guest location determined by SCXRD, drawn with thermal ellipsoids at probability 30%) and high temperature (several most possible locations were derived from molecular dynamic calculations, because guest location cannot be determined by SCXRD) phases of MCF-34·DMF. Hydrogen atoms are omitted for clarity.

5.2 Guest-controlled spin crossover

Tuning the magnetic behaviours of PCPs by guest molecules is a fascinating issue. Compared with other magnetic properties, SCO often occurs at relatively high temperatures, accompanying obvious variations of coordination configuration (usually the coordination bond length), which are generally studied by SCXRD. For examples, Kepert *et al*. reported guest-controlled SCO behaviours in a series of nanoporous frameworks $[Fe(NCS)_2(bpys)_2]$·guest (bpys = bipyridyl-type ligands) with diagonally 2-fold interpenetrated rhombic-grid structures and 1D channels.[183-187] Variable-temperature SCXRD measurements not only confirmed the significant length changes of Fe(II)–N coordination bonds at respective temperatures, but also revealed that the guest molecules can influence the spin states of Fe(II) ions by forming hydrogen-bonding interactions with the dipyridyl ligands, thiocyanate, and/or changing intraframework and extraframework supramolecular interactions.
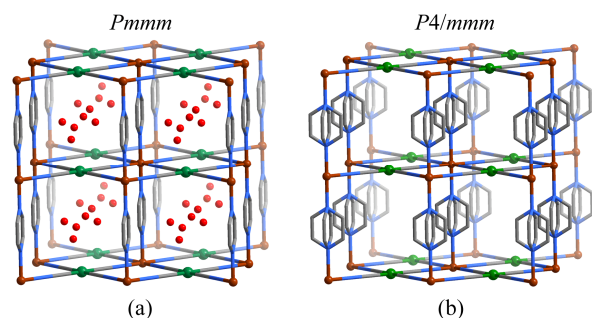
Fig. 35 The single-crystal structures of (a) $[Fe(pz)Ni(CN)_4]$·2H$_2$O and (b) $[Fe(pz)Ni(CN)_4]$. Note that the pz ligands are ordered in the orthorhombic structure (but the lattice H$_2$O molecules are disordered) but symmetrically disordered in the tetragonal structure. Hydrogen atoms are omitted for clarity.

The porous pillared-Hofmann-type frameworks $[FeM(CN)_4(pz)]$ (M = Ni, Pt; pz = pyrazine) with tetragonal structure is another notable system for guest-controlled SCO behaviours. For example, Kepert *et al*. showed that both the SCO transition temperatures and hysteresis widths of $[FeNi(CN)_4(pz)]$ can be tuned by H$_2$O inclusion.[188] Compared with the hydrated crystal $[FeNi(CN)_4(pz)]$·2H$_2$O, the guest-free crystal $[FeNi(CN)_4(pz)]$ has higher SCO transition temperature and wider hysteresis. A hydrated crystal mounted in an open-ended capillary was used for *in-situ* dehydration and SCXRD study. $[FeNi(CN)_4(pz)]$·2H$_2$O and $[FeNi(CN)_4(pz)]$ adopted the orthorhombic space group *Pmmm* and the tetragonal space group *P4/mmm*, respectively (Fig. 35). The change of crystal symmetry was attributed to the rotation of the pyrazine pillars in the more open space induced by the removal of lattice H$_2$O guest. The Fe(II)–N bond lengths of $[FeNi(CN)_4(pz)]$·2H$_2$O at 300 K (2.128(4)-2.226(6) Å) and 150 K (1.946(5)-1.971(5) Å) were consistent with the high-spin (HS) and low-spin (LS) states of Fe(II), respectively. Due to the very short bridging

ligands, the unit-cell volume of $[FeNi(CN)_4(pz)]$·2H$_2$O increased 15% from LS to HS. Although the H$_2$O molecules were disordered in $[FeNi(CN)_4(pz)]$·2H$_2$O, the observed relatively short OH$_2$···π(pz) contacts (3.56 Å) could be still indicative, which not only reduced the electron density of the pz ligands but also expanded the host framework to destabilize the LS state and decrease the SCO transition temperature. It should be noted that the orthorhombic phase exhibits pseudo-merohedral twining, which is common for structures with slightly distorted tetragonal topologies. During SCXRD analysis, the orthorhombic structure might be wrongly treated as a tetragonal structure. Nevertheless, PXRD showed that $[FeNi(CN)_4(pz)]$·2H$_2$O possessed a disordered tetragonal *P4/m* structure,[189] which was not consistent with SCO behaviours.[188]
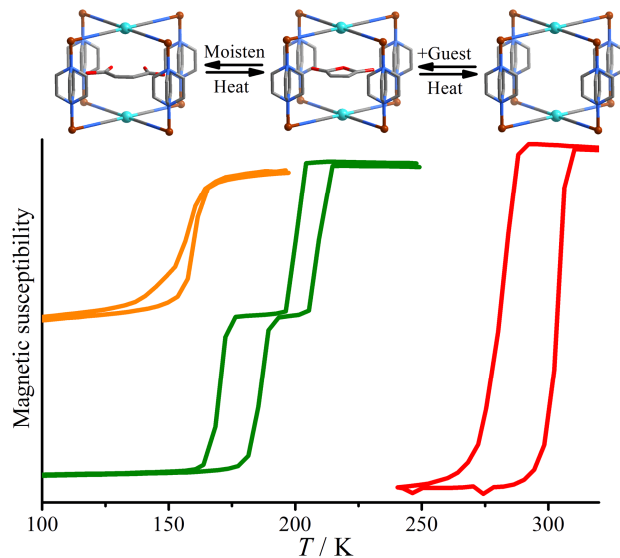
Fig. 36 Host-guest structures and temperature-dependent magnetic susceptibilities of $[FePt(CN)_4(pz)]$·0.9C$_4$H$_4$O$_4$·H$_2$O, $[FePt(CN)_4(pz)]$·0.9C$_4$H$_2$O$_3$·H$_2$O, and $[FePt(CN)_4(pz)]$. Note that the probable guest locations were derived from the residual electron density maps, and all three crystal structures adopt the disordered tetragonal structure. Hydrogen atoms are omitted for clarity.

Tong *et al*. successfully used an active guest to modify the SCO property of another porous pillared-Hofmann-type framework $[FePt(CN)_4(pz)]$.[190] The vacant crystal $[FePt(CN)_4(pz)]$ exhibited one-step SCO from fully HS and fully LS with a large hysteresis near room temperature. On the other hand, $[FePt(CN)_4(pz)]$·0.9C$_4$H$_2$O$_3$·H$_2$O (C$_4$H$_2$O$_3$ = maleic anhydride) showed two-step SCO from fully HS to 1:1 HS/LS and further to fully LS with smaller hystereses at lower temperatures, while $[FePt(CN)_4(pz)]$·0.9C$_4$H$_4$O$_4$·H$_2$O (C$_4$H$_4$O$_4$ = maleic acid) showed one-step SCO from fully HS to 1:1 HS/LS with even smaller hysteresis and lower temperature (Fig. 36). $[FePt(CN)_4(pz)]$·0.9C$_4$H$_2$O$_3$·H$_2$O and $[FePt(CN)_4(pz)]$·0.9C$_4$H$_4$O$_4$·H$_2$O can be interconverted to each other by moistening and heating the crystals, respectively. SCXRD showed that $[FePt(CN)_4(pz)]$·0.9C$_4$H$_2$O$_3$·H$_2$O and $[FePt(CN)_4(pz)]$·0.9C$_4$H$_4$O$_4$·H$_2$O possessed the same tetragonal space group *P4/mmm* with only one independent Fe(II) centre at all representative temperatures. The Fe–N bond lengths of the 1:1 HS/LS states were in between those for fully HS and LS states. Although variable temperature infrared spectroscopy indicated local structural rearrangement in $[FePt(CN)_4(pz)]$·0.9C$_4$H$_2$O$_3$·H$_2$O, no crystallographic evidence

for symmetry breaking was observed for the half high-spin states. The guest molecules were highly disordered in the crystal structures, so that the reversible transformation between maleic anhydride and maleic acid was monitored by infrared spectroscopy. Nevertheless, from the contour maps of the residual electron density, the molecular planes of maleic anhydride and maleic acid were observed to be parallel to the sheets. The larger guests unfavorable for the framework contraction can stabilize the HS states, resulting in the lower transition temperatures and incomplete transition behaviours.
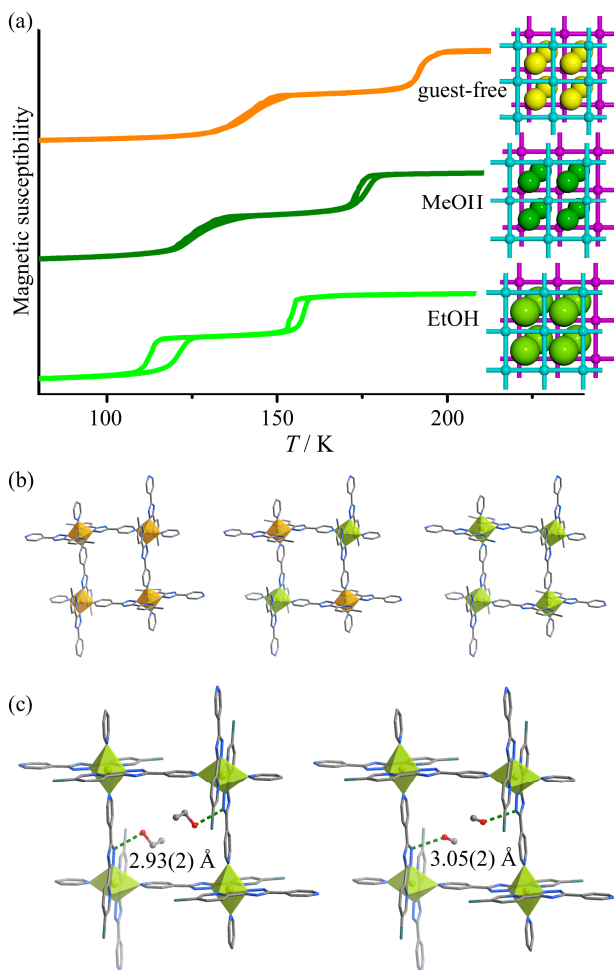
Fig. 37 (a) Temperature-dependent magnetic susceptibilities of [Fe(bdpt)$_2$], [Fe(bdpt)$_2$]·MeOH, and [Fe(bdpt)$_2$]·EtOH. (b) Single-crystal structures of the fully LS (left), 1:1 HS/LS (middle), and fully HS (right) states of [Fe(bdpt)$_2$]. (c) Single-crystal structures of [Fe(bdpt)$_2$]·EtOH and [Fe(bdpt)$_2$]·MeOH measured at 293 K. The HS and LS Fe(II) centers are shown as light-green and orange octahedra, respectively. Hydrogen atoms are omitted for clarity.

We observed well-defined guest-controlled two-step SCO behaviours and crystallographic data in [Fe(bdpt)$_2$]·guest (Hbdpt = 3-(5-bromo-2-pyridyl)-5-(4-pyridyl)-1,2,4-triazole, guest = Null, MeOH, or EtOH) consisting of offset packing square grids (Fig. 37). The guest-free crystal [Fe(bdpt)$_2$] was obtained by desolvation treatment of the as-synthesized sample [Fe(bdpt)$_2$]·EtOH or [Fe(bdpt)$_2$]·MeOH. All three phases showed two-step SCO behaviours, in which the transition temperatures ([Fe(bdpt)$_2$]·EtOH < [Fe(bdpt)$_2$]·MeOH < [Fe(bdpt)$_2$]) and hysteresis widths ([Fe(bdpt)$_2$]·EtOH >

[Fe(bdpt)$_2$]·MeOH > [Fe(bdpt)$_2$] ≈ 0) followed the sizes of the guests. SCXRD data of these compounds were collected at representative temperatures. The HS and LS states possessed the monoclinic space group $P2_1/n$, with only a single type of Fe(II) centres with characteristic Fe-N bond lengths. The space group changed to P-1 in the intermediate (1:1 HS/LS) states, giving two types of Fe(II) centres corresponding to the HS and LS states, respectively. It should be noted that, the lower-symmetry intermediate phases exhibited intrinsic twinning with unit-cell parameters very similar to those of the higher-symmetry, pure HS/LS phases. During SCXRD analysis of the intermediate phases, the diffraction pattern must be carefully handled as 50:50 twinning components to obtain the correct P-1 structures. Otherwise, the diffraction pattern could be also well processed and solved in the monoclinic space group $P2_1/n$ with only one type of mixed-spin Fe(II) centre. The guest molecules were well-resolved in the small cages, although they were 2-fold disordered due to the crystal symmetry. Well-defined host−guest hydrogen-bonding interactions between alcohol and uncoordinated nitrogen atoms of the triazolate ligands were observed. The O−H···N hydrogen-bond lengths were 2.93(2) and 3.05(2) Å for EtOH and MeOH, respectively, meaning that EtOH formed stronger hydrogen bonds with the host and reduced the electron density of the triazolate ligands, which lowered the transition temperature and increased the hysteresis widths.

6. Conclusions

As shown by the examples discussed above, beyond the routine structural characterization of the as-synthesized structures of crystalline materials, SCXRD has demonstrated significant advantages in the monitoring and explanation for structural transformations of PCPs induced by various types of chemical and physical stimuli, especially for those involving complicated host-guest structural information and small yet important structural alternations. Besides the elucidation of the adsorption affinity/preference of different sites and/or functional groups on the pore surface for gas absorption, SCXRD can also have other interesting applications. For instance, Fujita *et al*. showed that the intermediates and products of organic reactions and even trace amount of analytes can be embedded in the single crystals of PCPs and directly visualized by SCXRD.[191-195] Of course, SCXRD also play similar roles in other single-crystalline materials such as nonporous coordination polymers and organic crystals, which can also have notable flexibilities and reactivities, although they are out of the scope of this review.

Meanwhile, it is usually a great challenge to keep the sample single-crystallinity after the dynamic processes of activation, adsorption, and/or reaction. Thanks to the rapid development of instrumental and structural solution techniques, PXRD is and will be more and more frequently utilized in revealing the structural changes of flexible crystalline materials. Nevertheless, SCXRD is still irreplaceable, because it requires much less factitious restraints in the structure refinement. One should also notice that crystallography is not as direct as usually considered. Actually, the basis of crystallography in solving chemical/materials challenges is always based on the knowledge about the chemical information or compositions of the crystal and/or the reaction system. Also, crystallography only observes long-range ordered/averaged, thermodynamically static structural information. As discussed in some examples above, crystallography is less useful and even useless for guest

molecules incompatible with the crystal symmetries, dynamically disordered guest molecules and framework components, amorphous and poorly crystalline states, non-periodic defects, *etc.*, which are also sometimes important in the structure transformation processes of PCPs. To address more challenging and more interesting questions and phenomena, an integration of crystallography with *in-situ* spectroscopic and other chemical analytical methods should be very important and promising. To date, the dynamic behaviours and involved mechanisms of flexible PCPs are still mostly rationalized by the structural differences between the thermodynamically stable structures of the initial and final states. In view of the rapid progress/changing of technology, X-ray diffraction should be expected to have a better time-resolution for direct observation of the dynamic process or time-dependent evolution of structural changes.

Acknowledgements

Notes and references

MOE Key Laboratory of Bioinorganic and Synthetic Chemistry, State Key Laboratory of Optoelectronic Materials and Technologies, School of Chemistry and Chemical Engineering, Sun Yat-Sen University, Guangzhou 510275, China. E-mail: zhangjp7@mail.sysu.edu.cn; cxm@mail.sysu.edu.cn

1 S. R. Batten, N. R. Champness, X. M. Chen, J. Garcia-Martinez, S. Kitagawa, L. Ohrstrom, M. O'Keeffe, M. P. Suh and J. Reedijk, *Pure Appl. Chem.*, 2013, **85**, 1715-1724.

2 S. Kitagawa, R. Kitaura and S. Noro, *Angew. Chem., Int. Ed.*, 2004, **43**, 2334-2375.

3 H. X. Deng, S. Grunder, K. E. Cordova, C. Valente, H. Furukawa, M. Hmadeh, F. Gandara, A. C. Whalley, Z. Liu, S. Asahina, H. Kazumori, M. O'Keeffe, O. Terasaki, J. F. Stoddart and O. M. Yaghi, *Science*, 2012, **336**, 1018-1023.

4 J. P. Zhang, A. X. Zhu, R. B. Lin, X. L. Qi and X. M. Chen, *Adv. Mater.*, 2011, **23**, 1268-1271.

5 T. Devic, P. Horcajada, C. Serre, F. Salles, G. Maurin, B. Moulin, D. Heurtaux, G. Clet, A. Vimont, J.-M. Grenèche, B. L. Ouay, F. Moreau, E. Magnier, Y. Filinchuk, J. Marrot, J.-C. Lavalley, M. Daturi and G. Férey, *J. Am. Chem. Soc.*, 2009, **132**, 1127-1136.

6 Y. Cui, Y. Yue, G. Qian and B. Chen, *Chem. Rev.*, 2011, **112**, 1126-1162.

7 S. Horike, D. Umeyama and S. Kitagawa, *Acc. Chem. Res.*, 2013, **46**, 2376-2384.

8 M. Kurmoo, *Chem. Soc. Rev.*, 2009, **38**, 1353-1379.

9 S. Horike, S. Shimomura and S. Kitagawa, *Nat. Chem.*, 2009, **1**, 695-704.

10 L. C. Lin, J. Kim, X. Kong, E. Scott, T. M. McDonald, J. R. Long, J. A. Reimer and B. Smit, *Angew. Chem., Int. Ed.*, 2013, **52**, 4410-4413.

11 W. S. Drisdell, R. Poloni, T. M. McDonald, J. R. Long, B. Smit, J. B. Neaton, D. Prendergast and J. B. Kortright, *J. Am. Chem. Soc.*, 2013, **135**, 18183-18190.

12 M.-A. Springuel-Huet, A. Nossov, Z. Adem, F. Guenneau, C. Volkringer, T. Loiseau, G. Férey and A. Gédéon, *J. Am. Chem. Soc.*, 2010, **132**, 11599-11607.

13 S. Bourrelly, B. Moulin, A. Rivera, G. Maurin, S. Devautour-Vinot, C. Serre, T. Devic, P. Horcajada, A. Vimont, G. Clet, M. Daturi, J.-C. Lavalley, S. Loera-Serna, R. Denoyel, P. L. Llewellyn and G. Férey, *J. Am. Chem. Soc.*, 2010, **132**, 9488-9498.

14 C. Volkringer, T. Loiseau, N. Guillou, G. Férey, E. Elkaim and A. Vimont, *Dalton Trans.*, 2009, 2241-2249.

15 M. Haouas, C. Volkringer, T. Loiseau, G. Férey and F. Taulelle, *Chem. Mater.*, 2012, **24**, 2462-2471.

16 W. L. Bragg, *Proc. R. Soc. A*, 1913, **89**, 248-277.

17 G. Férey, C. Serre, C. Mellot-Draznieks, F. Millange, S. Surble, J. Dutour and I. Margiolaki, *Angew. Chem., Int. Ed.*, 2004, **43**, 6296-6301.

18 P. K. Allan, K. W. Chapman, P. J. Chupas, J. A. Hriljac, C. L. Renouf, T. C. A. Lucas and R. E. Morris, *Chem. Sci.*, 2012, **3**, 2559-2564.

19 M. Kawano and M. Fujita, *Coord. Chem. Rev.*, 2007, **251**, 2592-2605.

20 J. J. Vittal, *Coord. Chem. Rev.*, 2007, **251**, 1781-1795.

21 M. P. Suh and Y. E. Cheon, *Aust. J. Chem.*, 2006, **59**, 605-612.

22 G. J. Halder and C. J. Kepert, *Aust. J. Chem.*, 2006, **59**, 597-604.

23 G. K. Kole and J. J. Vittal, *Chem. Soc. Rev.*, 2013, **42**, 1755-1775.

24 S. Furukawa, Y. Sakata and S. Kitagawa, *Chem. Lett.*, 2013, **42**, 570-576.

25 G. Ferey and C. Serre, *Chem. Soc. Rev.*, 2009, **38**, 1380-1399.

26 S. Kitagawa and K. Uemura, *Chem. Soc. Rev.*, 2005, **34**, 109-119.

27 S. Kitagawa and R. Matsuda, *Coord. Chem. Rev.*, 2007, **251**, 2490-2509.

28 R. Medishetty, D. Jung, X. K. Song, D. Kim, S. S. Lee, M. S. Lah and J. J. Vittal, *Inorg. Chem.*, 2013, **52**, 2951-2957.

29 K. Biradha, Y. Hongo and M. Fujita, *Angew. Chem., Int. Ed.*, 2002, **41**, 3395-3398.

30 J.-P. Zhang, X.-C. Huang and X.-M. Chen, *Chem. Soc. Rev.*, 2009, **38**, 2385-2396.

31 D. Liu, M. Li and D. Li, *Chem. Commun.*, 2009, 6943-6945.

32 B. Zhang, D. Zhu and Y. Zhang, *Chem. Eur. J.*, 2010, **16**, 9994-9997.

33 A. Aslani and A. Morsali, *Chem. Commun.*, 2008, 3402-3404.

34 X.-N. Cheng, W.-X. Zhang and X.-M. Chen, *J. Am. Chem. Soc.*, 2007, **129**, 15738-15739.

35 D.-X. Xue, W.-X. Zhang, X.-M. Chen and H.-Z. Wang, *Chem. Commun.*, 2008, 1551-1553.

36 X.-M. Liu, B.-Y. Wang, W. Xue, L.-H. Xie, W.-X. Zhang, X.-N. Cheng and X.-M. Chen, *Dalton Trans.*, 2012, **41**, 13741-13746.

37 S. K. Ghosh, J.-P. Zhang and S. Kitagawa, *Angew. Chem., Int. Ed.*, 2007, **46**, 7965-7968.

38 S. K. Ghosh, W. Kaneko, D. Kiriya, M. Ohba and S. Kitagawa, *Angew. Chem., Int. Ed.*, 2008, **47**, 8843-8847.

39 W. Kaneko, M. Ohba and S. Kitagawa, *J. Am. Chem. Soc.*, 2007, **129**, 13706-13712.

40 S. B. Choi, H. Furukawa, H. J. Nam, D. Y. Jung, Y. H. Jhon, A. Walton, D. Book, M. O'Keeffe, O. M. Yaghi and J. Kim, *Angew. Chem., Int. Ed.*, 2012, **51**, 8791-8795.

41 L. Wen, P. Cheng and W. Lin, *Chem. Commun.*, 2012, **48**, 2846-2848.

42 Q. Chen, Z. Chang, W. C. Song, H. Song, H. B. Song, T. L. Hu and X. H. Bu, *Angew. Chem., Int. Ed.*, 2013, **52**, 11550-11553.

43 M. H. Zeng, S. Hu, Q. Chen, G. Xie, Q. Shuai, S. L. Gao and L. Y. Tang, *Inorg. Chem.*, 2009, **48**, 7070-7079.

44 B. Manna, A. K. Chaudhari, B. Joarder, A. Karmakar and S. K. Ghosh, *Angew. Chem., Int. Ed.*, 2013, **52**, 998-1002.

45 D. Bradshaw, J. E. Warren and M. J. Rosseinsky, *Science*, 2007, **315**, 977-980.

46 L.-H. Xie, J.-B. Lin, X.-M. Liu, Y. Wang, W.-X. Zhang, J.-P. Zhang and X.-M. Chen, *Inorg. Chem.*, 2010, **49**, 1158-1165.

47 C.-F. Zhuang, J. Zhang, Q. Wang, Z.-H. Chu, D. Fenske and C.-Y. Su, *Chem. Eur. J.*, 2009, **15**, 7578-7585.

48 Q. Chen, J. B. Lin, W. Xue, M. H. Zeng and X. M. Chen, *Inorg. Chem.*, 2011, **50**, 2321-2328.

49 J. Zhang, R. Liu, P. Feng and X. Bu, *Angew. Chem., Int. Ed.*, 2007, **46**, 8388-8391.

50 X. N. Cheng, W. X. Zhang, Y. Y. Lin, Y. Z. Zheng and X. M. Chen, *Adv. Mater.*, 2007, **19**, 1494-1498.

51 L.-H. Xie, Y. Wang, X.-M. Liu, J.-B. Lin, J.-P. Zhang and X.-M. Chen, *CrystEngComm*, 2011, **13**, 5849-5857.

52 A. S. R. Chesman, D. R. Turner, G. B. Deacon and S. R. Batten, *Chem. Commun.*, 2010, **46**, 4899-4901.

53 D. Braga, L. Maini, P. P. Mazzeo and B. Ventura, *Chem. Eur. J.*, 2010, **16**, 1553-1559.

54 J.-P. Zhang, Y.-Y. Lin, W.-X. Zhang and X.-M. Chen, *J. Am. Chem. Soc.*, 2005, **127**, 14162-14163.

55 X.-D. Chen, X.-H. Zhao, M. Chen and M. Du, *Chem. Eur. J.*, 2009, **15**, 12974-12977.

56 J. Seo, C. Bonneau, R. Matsuda, M. Takata and S. Kitagawa, *J. Am. Chem. Soc.*, 2011, **133**, 9005-9013.

57 J. Zhang and X. Bu, *Angew. Chem., Int. Ed.*, 2007, **46**, 6115-6118.

58 T. K. Maji, K. Uemura, H.-C. Chang, R. Matsuda and S. Kitagawa, *Angew. Chem., Int. Ed.*, 2004, **43**, 3269-3272.

59 K. Biradha and M. Fujita, *Angew. Chem., Int. Ed.*, 2002, **41**, 3392-3395.

60 F. Millange, C. Serre, N. Guillou, G. Férey and R. I. Walton, *Angew. Chem., Int. Ed.*, 2008, **47**, 4100-4105.

61 C. Serre, C. Mellot-Draznieks, S. Surble, N. Audebrand, Y. Filinchuk and G. Férey, *Science*, 2007, **315**, 1828-1831.

62 P. Horcajada, C. Serre, G. Maurin, N. A. Ramsahye, F. Balas, M. a. Vallet-Regí, M. Sebban, F. Taulelle and G. Férey, *J. Am. Chem. Soc.*, 2008, **130**, 6774-6780.

63 X.-M. Zhang, Y.-Z. Zheng, C.-R. Li, W.-X. Zhang and X.-M. Chen, *Cryst. Growth Des.*, 2007, **7**, 980-983.

64 Y.-S. Wei, K.-J. Chen, P.-Q. Liao, B.-Y. Zhu, R.-B. Lin, H.-L. Zhou, B.-Y. Wang, W. Xue, J.-P. Zhang and X.-M. Chen, *Chem. Sci.*, 2013, **4**, 1539-1546.

65 J. Jia, X. Lin, C. Wilson, A. J. Blake, N. R. Champness, P. Hubberstey, G. Walker, E. J. Cussen and M. Schröder, *Chem. Commun.*, 2007, 840-842.

66 R. I. Walton, A. S. Munn, N. Guillou and F. Millange, *Chem. Eur. J.*, 2011, **17**, 7069-7079.

67 T. Devic, P. Horcajada, C. Serre, F. Salles, G. Maurin, B. Moulin, D. Heurtaux, G. Clet, A. Vimont, J.-M. Grenèche, B. L. Ouay, F. Moreau, E. Magnier, Y. Filinchuk, J. Marrot, J.-C. Lavalley, M. Daturi and G. Férey, *J. Am. Chem. Soc.*, 2010, **132**, 1127-1136.

68 A. Demessence and J. R. Long, *Chem. Eur. J.*, 2010, **16**, 5902-5908.

69 J. Xiao, Y. Wu, M. Li, B.-Y. Liu, X.-C. Huang and D. Li, *Chem. Eur. J.*, 2013, **19**, 1891-1895.

70 X.-M. Zhang, Z.-M. Hao, W.-X. Zhang and X.-M. Chen, *Angew. Chem., Int. Ed.*, 2007, **46**, 3456-3459.

71 H. J. Choi, M. Dincă and J. R. Long, *J. Am. Chem. Soc.*, 2008, **130**, 7848-7850.

72 H. J. Choi, M. Dinca, A. Dailly and J. R. Long, *Energy Environ. Sci*, 2010, **3**, 117-123.

73 S. Galli, N. Masciocchi, V. Colombo, A. Maspero, G. Palmisano, F. J. López-Garzón, M. Domingo-García, I. Fernández-Morales, E. Barea and J. A. R. Navarro, *Chem. Mater.*, 2010, **22**, 1664-1672.

74 J.-P. Zhang and X.-M. Chen, *J. Am. Chem. Soc.*, 2008, **130**, 6010-6017.

75 B. Joarder, A. K. Chaudhari, S. S. Nagarkar, B. Manna and S. K. Ghosh, *Chem. Eur. J.*, 2013, **19**, 11178-11183.

76 Y. Sakata, S. Furukawa, M. Kondo, K. Hirai, N. Horike, Y. Takashima, H. Uehara, N. Louvain, M. Meilikhov, T. Tsuruoka, S. Isoda, W. Kosaka, O. Sakata and S. Kitagawa, *Science*, 2013, **339**, 193-196.

77 Y. Takashima, V. M. Martínez, S. Furukawa, M. Kondo, S. Shimomura, H. Uehara, M. Nakahama, K. Sugimoto and S. Kitagawa, *Nat. Commun.*, 2011, **2**, 168.

78 R. Kitaura, K. Seki, G. Akiyama and S. Kitagawa, *Angew. Chem., Int. Ed.*, 2003, **42**, 428-431.

79 M.-H. Zeng, X.-L. Feng and X.-M. Chen, *Dalton Trans.*, 2004, 2217-2223.

80 R. Yang, L. Li, Y. Xiong, J.-R. Li, H.-C. Zhou and C.-Y. Su, *Chem. Asian J.*, 2010, **5**, 2358-2368.

81 S. Yang, X. Lin, W. Lewis, M. Suyetin, E. Bichoutskaia, J. E. Parker, C. C. Tang, D. R. Allan, P. J. Rizkallah, P. Hubberstey, N. R. Champness, K. Mark Thomas, A. J. Blake and M. Schröder, *Nat. Mater.*, 2012, **11**, 710-716.

82 J.-P. Zhang, S. Horike and S. Kitagawa, *Angew. Chem., Int. Ed.*, 2007, **46**, 889-892.

83 J.-P. Zhang and S. Kitagawa, *J. Am. Chem. Soc.*, 2008, **130**, 907-917.

84 X.-L. Qi, R.-B. Lin, Q. Chen, J.-B. Lin, J.-P. Zhang and X.-M. Chen, *Chem. Sci.*, 2011, **2**, 2214-2218.

85 P. K. Allan, B. Xiao, S. J. Teat, J. W. Knight and R. E. Morris, *J. Am. Chem. Soc.*, 2010, **132**, 3605-3611.

86 B. D. Chandler, G. D. Enright, K. A. Udachin, S. Pawsey, J. A. Ripmeester, D. T. Cramb and G. K. Shimizu, *Nat. Mater.*, 2008, **7**, 229-235.

87 H. Wang, K. Yao, Z. Zhang, J. Jagiello, Q. Gong, Y. Han and J. Li, *Chem. Sci.*, 2014, **5**, 620-624.

88 D.-D. Zhou, C.-T. He, P.-Q. Liao, W. Xue, W.-X. Zhang, H.-L. Zhou, J.-P. Zhang and X.-M. Chen, *Chem. Commun.*, 2013, **49**, 11728-11730.

89 J.-B. Lin, J.-P. Zhang and X.-M. Chen, *J. Am. Chem. Soc.*, 2010, **132**, 6654-6656.

90 K. Lee, W. C. Isley Iii, A. L. Dzubak, P. Verma, S. J. Stoneburner, L.-C. Lin, J. D. Howe, E. D. Bloch, D. A. Reed, M. R. Hudson, C. M. Brown, J. R. Long, J. B. Neaton, B. Smit, C. J. Cramer, D. G. Truhlar and L. Gagliardi, *J. Am. Chem. Soc.*, 2013.

91 Y. Kubota, M. Takata, R. Matsuda, R. Kitaura, S. Kitagawa, K. Kato, M. Sakata and T. C. Kobayashi, *Angew. Chem., Int. Ed.*, 2005, **44**, 920-923.

92 L. J. Murray, M. Dinca, J. Yano, S. Chavan, S. Bordiga, C. M. Brown and J. R. Long, *J. Am. Chem. Soc.*, 2010, **132**, 7856-7857.

93 S. Xiang, Y. He, Z. Zhang, H. Wu, W. Zhou, R. Krishna and B. Chen, *Nat. Commun.*, 2012, **3**, 954.

94 R. Kitaura, S. Kitagawa, Y. Kubota, T. C. Kobayashi, K. Kindo, Y. Mita, A. Matsuo, M. Kobayashi, H. C. Chang, T. C. Ozawa, M. Suzuki, M. Sakata and M. Takata, *Science*, 2002, **298**, 2358-2361.

95 R. Matsuda, R. Kitaura, S. Kitagawa, Y. Kubota, R. V. Belosludov, T. C. Kobayashi, H. Sakamoto, T. Chiba, M. Takata, Y. Kawazoe and Y. Mita, *Nature*, 2005, **436**, 238-241.

96 J. L. C. Rowsell, E. C. Spencer, J. Eckert, J. A. K. Howard and O. M. Yaghi, *Science*, 2005, **309**, 1350-1354.

97 H. Sato, W. Kosaka, R. Matsuda, A. Hori, Y. Hijikata, R. V. Belosludov, S. Sakaki, M. Takata and S. Kitagawa, *Science*, 2013.

98 S. Yang, J. Sun, A. J. Ramirez-Cuesta, S. K. Callear, I. F. DavidWilliam, D. P. Anderson, R. Newby, A. J. Blake, J. E. Parker, C. C. Tang and M. Schröder, *Nat. Chem.*, 2012, **4**, 887-894.

99 J. Seo, R. Matsuda, H. Sakamoto, C. Bonneau and S. Kitagawa, *J. Am. Chem. Soc.*, 2009, **131**, 12792-12800.

100 S. R. Miller, P. A. Wright, T. Devic, C. Serre, G. r. Férey, P. L. Llewellyn, R. Denoyel, L. Gaberova and Y. Filinchuk, *Langmuir*, 2009, **25**, 3618-3626.

101 J. B. Lin, W. Xue, J. P. Zhang and X. M. Chen, *Chem. Commun.*, 2011, **47**, 926-928.

102 A. M. Plonka, D. Banerjee, W. R. Woerner, Z. Zhang, N. Nijem, Y. J. Chabal, J. Li and J. B. Parise, *Angew. Chem., Int. Ed.*, 2013, **52**, 1692-1695.

103 M. Dinca, W. S. Han, Y. Liu, A. Dailly, C. M. Brown and J. R. Long, *Angew. Chem., Int. Ed.*, 2007, **46**, 1419-1422.

104 J.-P. Zhang and X.-M. Chen, *J. Am. Chem. Soc.*, 2009, **131**, 5516-5521.

105 R. Vaidhyanathan, S. S. Iremonger, G. K. Shimizu, P. G. Boyd, S. Alavi and T. K. Woo, *Science*, 2010, **330**, 650-653.

106 S. Takamizawa, T. Hiroki, E. Nakata, K. Mochizuki and W. Mori, *Chem. Lett.*, 2002, 1208-1209.

107 S. Takamizawa, E.-i. Nataka, T. Akatsuka, R. Miyake, Y. Kakizaki, H. Takeuchi, G. Maruta and S. Takeda, *J. Am. Chem. Soc.*, 2010, **132**, 3783-3792.

108 S. Takamizawa, E.-i. Nakata, H. Yokoyama, K. Mochizuki and W. Mori, *Angew. Chem., Int. Ed.*, 2003, **115**, 4467-4470.

109 S. Takamizawa, Y. Takasaki and R. Miyake, *Chem. Commun.*, 2009, 6625-6627.

110 C. Kachi-Terajima, T. Akatsuka, M.-a. Kohbara and S. Takamizawa, *Chem. Asian J.*, 2007, **2**, 40-50.

111 S. Takamizawa, E.-i. Nakata and R. Miyake, *Dalton Trans.*, 2009, 1752-1760.

112 S. Takamizawa, E.-i. Nakata and T. Saito, *Angew. Chem., Int. Ed.*, 2004, **43**, 1368-1371.

113 S. Takamizawa and M.-a. Kohbara, *Dalton Trans.*, 2007, 3640-3645.

114 S. Takamizawa and E.-i. Nakata, *CrystEngComm*, 2005, **7**, 476-479.

115 M. Dinca, W. S. Han, Y. Liu, A. Dailly, C. M. Brown and J. R. Long, *Angew. Chem., Int. Ed.*, 2007, **46**, 1419-1422.

116 P.-Q. Liao, D.-D. Zhou, A.-X. Zhu, L. Jiang, R.-B. Lin, J.-P. Zhang and X.-M. Chen, *J. Am. Chem. Soc.*, 2012, **134**, 17380-17383.

117 T. K. Maji, G. Mostafa, R. Matsuda and S. Kitagawa, *J. Am. Chem. Soc.*, 2005, **127**, 17152-17153.

118 X.-C. Huang, *PhD Thesis*, Sun Yat-Sen University, 2004.

119 X. C. Huang, Y. Y. Lin, J. P. Zhang and X. M. Chen, *Angew. Chem., Int. Ed.*, 2006, **45**, 1557-1559.

120 K. S. Park, Z. Ni, A. P. Côté, J. Y. Choi, R. Huang, F. J. Uribe-Romo, H. K. Chae, M. O'Keeffe and O. M. Yaghi, *Proc. Natl. Acad. Sci. U. S. A.*, 2006, **103**, 10186-10191.

121 P. Van Der Sluis and A. L. Spek, *Acta Crystallogr. A*, 1990, **46**, 194-201.

122 S. A. Moggach, T. D. Bennett and A. K. Cheetham, *Angew. Chem., Int. Ed.*, 2009, **48**, 7087-7089.

123 D. Fairen-Jimenez, S. A. Moggach, M. T. Wharmby, P. A. Wright, S. Parsons and T. Düren, *J. Am. Chem. Soc.*, 2011, **133**, 8900-8902.

124 J. P. Zhang, A. X. Zhu and X. M. Chen, *Chem. Commun.*, 2012, **48**, 11395-11397.

125 C. Yang, X. Wang and M. A. Omary, *J. Am. Chem. Soc.*, 2007, **129**, 15454-15455.

126 C. Yang, X. Wang and M. A. Omary, *Angew. Chem., Int. Ed.*, 2009, **48**, 2500-2505.

127 S. M. Cohen, *Chem. Rev.*, 2011, **112**, 970-1000.

128 S. M. Cohen, *Chem. Sci.*, 2010, **1**, 32-36.

129 K. K. Tanabe and S. M. Cohen, *Chem. Soc. Rev.*, 2011, **40**, 498-519.

130 Z. Wang and S. M. Cohen, *Chem. Soc. Rev.*, 2009, **38**, 1315-1329.

131 J. M. Falkowski, C. Wang, S. Liu and W. Lin, *Angew. Chem., Int. Ed.*, 2011, **50**, 8674-8678.

132 I.-H. Park, A. Chanthapally, Z. Zhang, S. S. Lee, M. J. Zaworotko and J. J. Vittal, *Angew. Chem., Int. Ed.*, 2014, **53**, 414-419.

133 M. Nagarathinam, A. M. P. Peedikakkal and J. J. Vittal, *Chem. Commun.*, 2008, 5277-5288.

134 R. Medishetty, L. L. Koh, G. K. Kole and J. J. Vittal, *Angew. Chem., Int. Ed.*, 2011, **50**, 10949-10952.

135 M. H. Mir, L. L. Koh, G. K. Tan and J. J. Vittal, *Angew. Chem., Int. Ed.*, 2010, **49**, 390-393.

136 Y.-C. Ou, D.-S. Zhi, W.-T. Liu, Z.-P. Ni and M.-L. Tong, *Chem. Eur. J.*, 2012, **18**, 7357-7361.

137 M.-H. Xie, X.-L. Yang and C.-D. Wu, *Chem. Eur. J.*, 2011, **17**, 11424-11427.

138 K. K. Tanabe, Z. Q. Wang and S. M. Cohen, *J. Am. Chem. Soc.*, 2008, **130**, 8508-8517.

139 Z. Q. Wang and S. M. Cohen, *Angew. Chem., Int. Ed.*, 2008, **47**, 4699-4702.

140 E. Dugan, Z. Q. Wang, M. Okamura, A. Medina and S. M. Cohen, *Chem. Commun.*, 2008, 3366-3368.

141 Z. Q. Wang, K. K. Tanabe and S. M. Cohen, *Inorg. Chem.*, 2009, **48**, 296-306.

142 Z. Wang and S. M. Cohen, *J. Am. Chem. Soc.*, 2007, **129**, 12368-12369.

143 A. D. Burrows, C. G. Frost, M. F. Mahon and C. Richardson, *Angew. Chem., Int. Ed.*, 2008, **47**, 8482-8486.

144 R. K. Deshpande, J. L. Minnaar and S. G. Telfer, *Angew. Chem., Int. Ed.*, 2010, **49**, 4598-4602.

145 H. Sato, R. Matsuda, K. Sugimoto, M. Takata and S. Kitagawa, *Nat. Mater.*, 2010, **9**, 661-666.

146 K. K. Tanabe, C. A. Allen and S. M. Cohen, *Angew. Chem., Int. Ed.*, 2010, **49**, 9730-9733.

147 B. J. Burnett, P. M. Barron, C. Hu and W. Choe, *J. Am. Chem. Soc.*, 2011, **133**, 9984-9987.

148 H. J. Park, Y. E. Cheon and M. P. Suh, *Chem. Eur. J.*, 2010, **16**, 11662-11669.

149 G. Mukherjee and K. Biradha, *Chem. Commun.*, 2012, **48**, 4293-4295.

150 M. Kim, J. F. Cahill, H. Fei, K. A. Prather and S. M. Cohen, *J. Am. Chem. Soc.*, 2012, **134**, 18082-18088.

151 C. K. Brozek and M. Dinca, *Chem. Sci.*, 2012, **3**, 2110-2113.

152 T. K. Prasad, D. H. Hong and M. P. Suh, *Chem. Eur. J.*, 2010, **16**, 14043-14050.

153 Q. Yao, J. Sun, K. Li, J. Su, M. V. Peskov and X. Zou, *Dalton Trans.*, 2012, **41**, 3953-3955.

154 N. Planas, A. L. Dzubak, R. Poloni, L.-C. Lin, A. McManus, T. M. McDonald, J. B. Neaton, J. R. Long, B. Smit and L. Gagliardi, *J. Am. Chem. Soc.*, 2013, **135**, 7402-7405.

155 Z. Zhang, L. Wojtas, M. Eddaoudi and M. J. Zaworotko, *J. Am. Chem. Soc.*, 2013, **135**, 5982-5985.

156 Z. Zhang, L. Zhang, L. Wojtas, P. Nugent, M. Eddaoudi and M. J. Zaworotko, *J. Am. Chem. Soc.*, 2012, **134**, 924-927.

157 S. Das, H. Kim and K. Kim, *J. Am. Chem. Soc.*, 2009, **131**, 3814-3815.

158 O. Karagiaridi, M. B. Lalonde, W. Bury, A. A. Sarjeant, O. K. Farha and J. T. Hupp, *J. Am. Chem. Soc.*, 2012, **134**, 18790-18796.

159 O. Karagiaridi, W. Bury, A. A. Sarjeant, C. L. Stern, O. K. Farha and J. T. Hupp, *Chem. Sci.*, 2012, **3**, 3256-3260.

160 T. Li, M. T. Kozlowski, E. A. Doud, M. N. Blakely and N. L. Rosi, *J. Am. Chem. Soc.*, 2013, **135**, 11688-11691.

161 P. V. Dau, M. Kim and S. M. Cohen, *Chem. Sci.*, 2013, **4**, 601-605.

162 L. Ma, C. D. Wu, M. M. Wanderley and W. Lin, *Angew. Chem., Int. Ed.*, 2010, **49**, 8244-8248.

163 S. Yang, X. Lin, A. J. Blake, G. S. Walker, P. Hubberstey, N. R. Champness and M. Schröder, *Nat. Chem.*, 2009, **1**, 487-493.

164 Z. Zhang, W. Y. Gao, L. Wojtas, S. Ma, M. Eddaoudi and M. J. Zaworotko, *Angew. Chem., Int. Ed.*, 2012, **51**, 9330-9334.

165 T. Jacobs, R. Clowes, A. I. Cooper and M. J. Hardie, *Angew. Chem., Int. Ed.*, 2012, **51**, 5192-5195.

166 M. Dinca, A. Dailly and J. R. Long, *Chem. – Eur. J.*, 2008, **14**, 10280-10285.

167 K. W. Chapman, P. J. Chupas and C. J. Kepert, *J. Am. Chem. Soc.*, 2005, **127**, 15630-15636.

168 A. L. Goodwin, M. Calleja, M. J. Conterio, M. T. Dove, J. S. O. Evans, D. A. Keen, L. Peters and M. G. Tucker, *Science*, 2008, **319**, 794-797.

169 S. Margadonna, K. Prassides and A. N. Fitch, *J. Am. Chem. Soc.*, 2004, **126**, 15390-15391.

170 K. W. Chapman, P. J. Chupas and C. J. Kepert, *J. Am. Chem. Soc.*, 2006, **128**, 7009-7014.

171 M. Brunelli, J. P. Wright, G. R. M. Vaughan, A. J. Mora and A. N. Fitch, *Angew. Chem., Int. Ed.*, 2003, **42**, 2029-2032.

172 J. M. Ogborn, I. E. Collings, S. A. Moggach, A. L. Thompson and A. L. Goodwin, *Chem. Sci.*, 2012, **3**, 3011-3017.

173 L. D. DeVries, P. M. Barron, E. P. Hurley, C. H. Hu and W. Choe, *J. Am. Chem. Soc.*, 2011, **133**, 14848-14851.

174 A. E. Phillips, G. J. Halder, K. W. Chapman, A. L. Goodwin and C. J. Kepert, *J. Am. Chem. Soc.*, 2010, **132**, 10-11.

175 Y. Wu, A. Kobayashi, G. J. Halder, V. K. Peterson, K. W. Chapman, N. Lock, P. D. Southon and C. J. Kepert, *Angew. Chem., Int. Ed.*, 2008, **47**, 8929-8932.

176 D. Dubbeldam, K. S. Walton, D. E. Ellis and R. Q. Snurr, *Angew. Chem., Int. Ed.*, 2007, **46**, 4496-4499.

177 N. Lock, Y. Wu, M. Christensen, L. J. Cameron, V. K. Peterson, A. J. Bridgeman, C. J. Kepert and B. B. Iversen, *J. Phys. Chem. C*, 2010, **114**, 16181-16186.

178 A. L. Goodwin, K. W. Chapman and C. J. Kepert, *J. Am. Chem. Soc.*, 2005, **127**, 17980-17981.

179 A. L. Spek, *J. Appl. Crystallogr.*, 2003, **36**, 7-13.

180 A. E. Phillips, A. L. Goodwin, G. J. Halder, P. D. Southon and C. J. Kepert, *Angew. Chem., Int. Ed.*, 2008, **47**, 1396-1399.

181 I. Grobler, V. J. Smith, P. M. Bhatt, S. A. Herbert and L. J. Barbour, *J. Am. Chem. Soc.*, 2013, **135**, 6411-6414.

182 H.-L. Zhou, R.-B. Lin, C.-T. He, Y.-B. Zhang, N. Feng, Q. Wang, F. Deng, J.-P. Zhang and X.-M. Chen, *Nat. Commun.*, 2013, **4**, 2534.

183 S. M. Neville, G. J. Halder, K. W. Chapman, M. B. Duriska, P. D. Southon, J. D. Cashion, J. F. Letard, B. Moubaraki, K. S. Murray and C. J. Kepert, *J. Am. Chem. Soc.*, 2008, **130**, 2869-2876.

184 S. M. Neville, G. J. Halder, K. W. Chapman, M. B. Duriska, B. Moubaraki, K. S. Murray and C. J. Kepert, *J. Am. Chem. Soc.*, 2009, **131**, 12106-12108.

185 G. J. Halder, C. J. Kepert, B. Moubaraki, K. S. Murray and J. D. Cashion, *Science*, 2002, **298**, 1762-1765.

186 S. M. Neville, B. Moubaraki, K. S. Murray and C. J. Kepert, *Angew. Chem., Int. Ed.*, 2007, **46**, 2059-2062.

187 G. J. Halder, K. W. Chapman, S. M. Neville, B. Moubaraki, K. S. Murray, J. F. Letard and C. J. Kepert, *J. Am. Chem. Soc.*, 2008, **130**, 17552-17562.

188 L. L. Peter D. Southon, Elizabeth A. Fellows, David J. Price, Gregory J. Halder, Karena W. Chapman, Boujemaa Moubaraki, Keith S. Murray, Jean-Francois Letard, and Cameron J. Kepert, *J. Am. Chem. Soc.*, 2009, **131**, 10998–11009.

189 V. Niel, J. M. Martinez-Agudo, M. C. Muñoz, A. B. Gaspar and J. A. Real, *Inorg. Chem.*, 2001, **40**, 3838-3839.

190 X. Bao, H. J. Shepherd, L. Salmon, G. Molnar, M. L. Tong and A. Bousseksou, *Angew. Chem., Int. Ed.*, 2013, **52**, 1198-1202.

191 K. Ikemoto, Y. Inokuma and M. Fujita, *Angew. Chem., Int. Ed.*, 2010, **49**, 5750-5752.

192 T. Kawamichi, Y. Inokuma, M. Kawano and M. Fujita, *Angew. Chem., Int. Ed.*, 2010, **49**, 2375-2377.

193 H. Tsuyoshi, K. Masaki, K. Takehide and M. Fujita, *J. Am. Chem. Soc.*, 2008, **130**, 15781579.

194 T. Kawamichi, T. Haneda, M. Kawano and M. Fujita, *Nature*, 2009, **461**, 633-635.

195 I. Yasuhide, K. Masaki and M. Fujita, *Nat. Chem.*, 2011, **3**, 349-358.

Table of contents
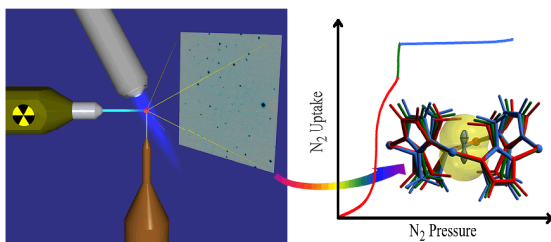
This review gives a brief overview of single-crystal X-ray diffraction studies and single-crystal to single-crystal transformations of porous coordination polymers.

Jie-Peng Zhang obtained his B.Sc. in 2000 and Ph.D. in 2005 under the supervision of Prof. X.-M. Chen at Sun Yat-Sen University (SYSU). He was a JSPS postdoc in Prof. S. Kitagawa's group at Kyoto University from 2005 to 2007. After that, he moved back and joined SYSU in 2007, and became a professor in 2011. His current research interest is in the chemistry of porous coordination polymers.

Pei-Qin Liao was born in Guangdong, China, in 1988. He received his B.Sc. in chemistry in 2011 from SYSU and then joined Prof. X.-M. Chen's group for his Ph.D. study. He is interested in the design, synthesis, and application of new porous materials.

Hao-Long Zhou was born in Guangdong, China, in 1989. He received his B.Sc. in chemistry in 2012 from SYSU. After that he joined Prof. X.-M. Chen's group for his Ph.D. study. His recent research interest focuses on the crystal engineering of flexible

porous coordination polymers

Rui-Biao Lin was born in Guangdong, China, in 1986. He received his B.Sc. in chemistry in 2009 from SYSU and then joined Prof. X.-M. Chen's group for his Ph.D. study, working in the synthesis, structures, and property studies of porous coordination polymers.

Xiao-Ming Chen obtained his B.Sc. in 1983 and M.Sc. under the supervision of Prof. H.-F. Fan in 1986 from SYSU, and his Ph.D. under the supervision of Prof. T. C. W. Mak at the Chinese University of Hong Kong in 1992. He then joined SYSU and became a professor in 1995. He was elected to CAS in 2009 and TWAS in 2013. His current research interest is in synthesis and crystal engineering of functional metal complexes and coordination polymers.